# THE GENERATION OF $T$ WAVES BY EARTHQUAKES

EMILE A. OKAL

*Department of Earth and Planetary Sciences, Northwestern University, Evanston, IL 60201, USA*

## ABSTRACT

$T$ waves propagate in the so-called SOFAR channel of minimum sound velocity acting as a waveguide for acoustic energy in the world's oceans. They can be excited by sources in the solid Earth such as earthquakes through conversion of seismic energy into acoustic waves at the solid–liquid interfaces. We present a historical perspective of the investigations of such conversions. In the context of geometrical optics, a sloping interface provides a mechanism for the penetration of the SOFAR channel after a series of reflections in the liquid wedge. This process, known as "downslope conversion", successfully explained many characteristics of earthquake-generated $T$ waves, but has severe limitations, notably regarding "abyssal" $T$ phases, generated under flat oceanic basins. We review theoretical developments based on mode theory which describe coupling between elastic and acoustic modes under scattering by structural heterogeneities located at the ocean bottom, and which are becoming increasingly successful at modeling the waveshapes of abyssal $T$ phases.

As a particular form of seismic wave emanating from an earthquake, $T$ waves can provide insight into seismic sources in the oceanic environment. We review the application of $T$ waves to the detection of small earthquakes in marine basins, discuss the retrieval of seismic source properties from $T$-phase waveforms, and show that several algorithms combining measurements of their amplitude and duration can yield information on source rupture, and more specifically detect the presence of source slowness. In particular, anomalously slow earthquakes such as the so-called "tsunami earthquakes" are poor $T$-wave generators, and more generally, $T$-phase amplitudes and tsunami generation are not found to correlate.

In the context of the Comprehensive Nuclear-Test Ban Treaty, hydroacoustics has been recognized as a monitoring technology, and the deployment of state-of-the-art receivers at eleven sites will significantly improve long-range detection capabilities and open up new opportunities for the investigation of acoustic sources, including earthquakes, in the oceanic environment.




ISSN: 0065-2687
DOI: 10.1016/S0065-2687(07)49001-X

## 1. Introduction

This paper examines the generation, by earthquake sources, of the so-called $T$ waves guided in the water body of the world's oceans through a channel of minimum sound velocity generally centered around 1200 meters depth. It discusses the mechanisms of conversion of elastic energy in the solid Earth into acoustic energy in the water, describes the potential for improving our knowledge of the seismicity of remote ocean provinces using $T$ waves, and shows that recent developments in the quantification of teleseismic $T$ phases can help shed new light on the high-frequency properties of earthquake source spectra.

The variation of sound velocity with depth in the ocean was originally investigated in order to convert shipboard acoustic measurements into accurate depth soundings (e.g., Langevin, 1924; Kuwahara, 1939). In simple terms, the velocity of acoustic waves in water is controlled by the thermodynamic variables describing its state, namely composition, pressure and temperature. Under ambient oceanic conditions, the sound velocity increases with pressure, at a rate of about $1.8 \times 10^{-6}$ m s$^{-1}$ Pa$^{-1}$, with temperature at a rate of 2.1 m s$^{-1}$ K$^{-1}$, and with salinity at a rate of 1.3 m s$^{-1}$ per part per 1000 (Sverdrup *et al.*, 1942). In the oceanic column, the pressure is hydrostatic, increasing linearly with depth, which translates into a positive velocity gradient of 0.018 s$^{-1}$, or 1.8 m/s per 100 m of oceanic column. The effect of temperature is far more complex, since the thermal gradient in the world's oceans is highly variable, both spatially and seasonally (Teague *et al.*, 1990; Levitus *et al.*, 1994). In most areas, the temperature drops significantly through the thermocline layer, and in particular in the first 150 m, and then much more slowly at greater depths. Salinity can have a highly variable behavior in the thermocline, and stabilizes around 35 parts per thousand in the deeper ocean. As a whole, the effect of temperature on sound velocity prevails in the thermocline and that of pressure in the deep ocean, creating a minimum in sound velocity at around 1200 m, where the resulting low-velocity channel can trap acoustic energy with wavelengths shorter than its width, in practice with frequencies greater than 2.5 Hz. The existence of this waveguide was recognized and its structure investigated early on (Swainson, 1936), but its full potential for efficient long-range propagation was realized and thoroughly studied only during World War II, as summarized upon post-war declassification by Ewing *et al.* (1946), who coined the acronym SOFAR (for **SO**und **F**ixing **A**nd **R**anging) for the technique and, by extension, for the low-velocity channel itself.

Irrespective of the presence of the SOFAR channel, it had long been recognized, apparently ever since Leonardo da Vinci (Urick, 1975), that the propagation of sound in water is particularly efficient, especially as compared to propagation in the atmosphere. Modern experimental research (Urick, 1963; Thorp, 1965; Urick, 1966) has indeed documented the virtual absence of anelastic attenuation in seawater in the 1–100 Hz frequency range, which serves to further enhance the

efficiency of the SOFAR channel, and sets the finite size of the ocean basins as the only physical limit to the range of SOFAR propagation.

Despite the variability of the detailed characteristics of the sound velocity profile (depth of SOFAR axis, minimum velocity, reciprocal depth, etc.), the existence of the channel is a quasi-universal feature, the only possible exceptions involving the cold waters of the extreme Southern Ocean from which the thermocline is absent. Its ability to propagate energy from exceptionally small sources over remarkably large distances has found applications world-wide in fields as varied as the tracking of submarines, the discovery and monitoring of distant volcanoes (Dietz and Sheehy, 1954; Norris and Johnson, 1969; Talandier and Okal, 1982, 1996; Fox *et al.*, 1995), the detection of explosions in the oceanic environment, notably in the context of the Comprehensive Nuclear-Test Ban Treaty (CTBT) (Milne, 1959; Adams, 1979; Okal, 2001a; Wallace and Koper, 2002; Reymond *et al.*, 2003; Talandier and Okal, 2004a), the detection of iceberg collisions in the Southern Ocean (Talandier *et al.* 2002; 2006), the study of the vocalization patterns of large cetaceans (Reysenbach de Haan, 1966; Stafford *et al.*, 1998), and the monitoring of global warming (Munk *et al.*, 1994).

While SOFAR propagation is limited to the oceanic column, acoustic energy in the water can be transformed to and from elastic energy at the solid–liquid interfaces marking the boundaries of an oceanic basin, and this mechanism, whose degree of complexity can vary widely, allows both the excitation of acoustic energy by sources in the solid Earth, such as earthquakes and underground explosions, and its recording by land-based seismic stations located near the shore or even, under exceptional circumstances, hundreds of kilometers away from the coastlines (Båth and Shahidi, 1971; Cansi and Béthoux, 1985; Pasyanos and Romanowicz, 1997). Indeed, when the seismic wave resulting from the receiver-side conversion is of sufficient amplitude, it can be felt by the population close to the shore, even though the source of the acoustic energy may be many thousands of kilometers away. Examples include the underwater nuclear explosion WIGWAM on 14 May 1955, felt in Hawaii (J.P. Eaton, pers. comm., 1979) and even in Torishima, 8750 km from the source (Wadati, 1960); the Fairweather, Alaska earthquake on 10 July 1958 felt in Hawaii (J.P. Eaton, pers. comm., Eaton, 1979); the Tonga earthquake on 22 June 1977 felt in Tahiti (Talandier and Okal, 1979); the South Island, New Zealand earthquake of 21 August 2003 felt in Sydney, Australia (Leonard, 2004); and as discussed below, the great 2004 Sumatra earthquake felt in the Maldives (A.C. Yalçıner, pers. comm., 2005). In addition, *T* waves from certain Venezuelan earthquakes are routinely felt in Puerto Rico at a somewhat shorter distance (not exceeding 900 km) (C.G. von Hillebrandt-Andrade, pers. comm., 1998). Note that coupling is also possible, at least in principle, with the atmospheric column; however, the mechanics of the conversion of air waves into acoustic phases are poorly understood, due to the scant number of adequate sources, consisting exclusively of large atmospheric nuclear tests in the early 1960s (Talandier and Okal, 2001, 2004b).

As discussed more in detail below, earthquake-generated hydroacoustic wavetrains were first identified as a far-field phase on seismograms (if not correctly interpreted) in 1935 by scientists at Harvard Observatory upon recording of Caribbean earthquakes (Collins, 1936), and given the name $T$ group (for "*Tertiary*" arrival, following $P$, primary and $S$, secondary) during informal discussions of these phases by the Harvard staff (Leet *et al.*, 1951). To our knowledge, this name first appeared in print in Linehan (1940).

When $T$ waves were later correctly identified as water-borne waves guided by the SOFAR channel, a major problem arose, as the excitation of $T$ waves trapped in the channel from earthquake sources located in the solid Earth, and thus by necessity outside the waveguide, is theoretically impossible in the framework of geometrical optics applied to a simple flat-layered Earth model. Indeed, all acceptable sound velocity profiles predict that only rays inclined less than $\sim 12°$ on the horizontal can be trapped in the channel, while the sharp contrast in seismic and acoustic velocities in the source region precludes the penetration of the oceanic column at all but the steepest incidences.

In this framework, the present paper offers a largely chronological review of five decades of observational developments and theoretical efforts, seeking to resolve the apparent paradox of the ubiquitous observation of efficient excitation and propagation of far-field $T$ phases from earthquake sources, through a series of modifications to the simple flat-layered model based on geometrical optics. It further discusses various efforts at quantifying the energy present in $T$ phases, including recent developments that use their characteristics to explore the dynamics of the seismic source.

The discussion of the excitation of $T$ waves by acoustic sources in the water column, such as man-made underwater explosions, magmatic episodes of volcanism delivering magma to the ocean floor, or the generation of cryosignals during collision between large icebergs, is intentionally left out of the present review.

## 2. Geometrical Optics: Understanding $T$ Waves in a Simple Context

### Early Observations

To our knowledge, the first published report of a teleseismic $T$ wavetrain goes back to Jaggar (1930), who describes high-frequency oscillations recorded at Hawaii Volcano Observatory (HVO) in the coda of a major earthquake which took place on 24 October 1927 on the Fairweather Fault of the Alaska panhandle (Fig. 1). However, Jaggar interprets the record as local volcanic tremor "possibly touched off by the big earthquake waves". A modern examination of the spindle-shaped waveform, frequency content and timing of the phase (quoted as 06:20 a.m. HST or 16:50 GMT) definitely identifies it as the $T$ wave of the

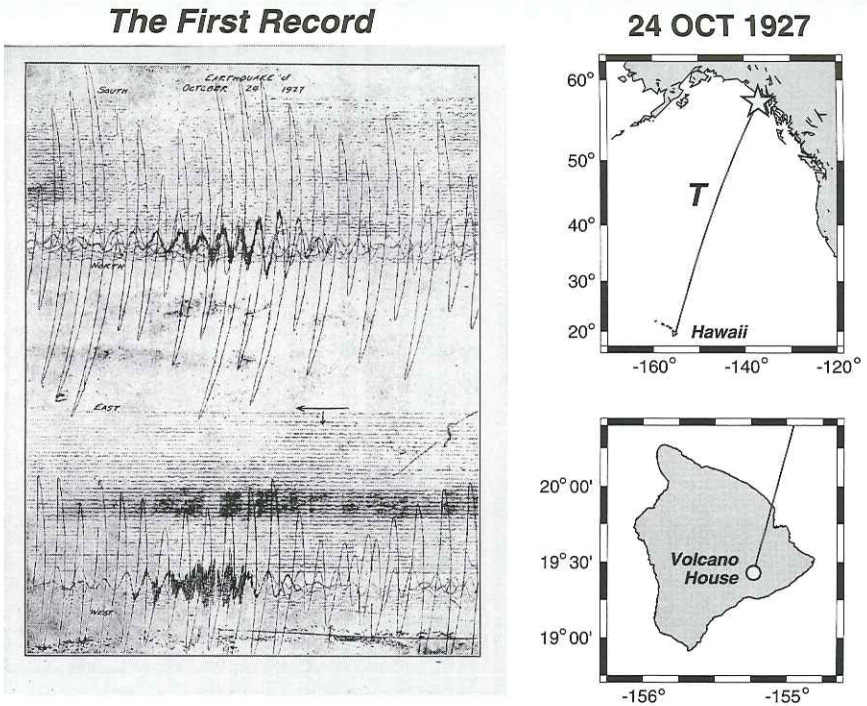


FIG. 1. *Left*: Seismic recording of the Alaskan earthquake of 24 October 1927 at Hawaii Volcano Observatory, after Jaggar (1930). This is believed to be the first published record of a teleseismic *T* phase. The top trace is the S–N component, the lower one, the E–W component; time increases from right to left and from top to bottom. The window is approximately 200 seconds long. *Right*: Maps sketching the transpacific path of the *T* phase from source (star) to receiver, and the location of the receiver station inside the "Big" Island of Hawaii. Adapted from Jaggar (1930).

Alaskan earthquake. Note that Jaggar mentions that the phase was "feebly felt" in Hawaii, as would later be the larger 1958 earthquake, in a very similar geometry.

Several years later, Collins (1936) noted in the Seismological Bulletin of Harvard Observatory that the record of the Caribbean earthquake of 15 September 1935 featured a third arrival, following $P$ and $S$, detected exclusively on short-period channels. This constitutes the first correct interpretation of a $T$ wave as the independent phase of a distant earthquake. Our relocation of that earthquake based on travel-times published in the International Seismological Summary (ISS) and the algorithm of Wysession *et al.* (1991) converges on 19.03°N, 64.85°W and a depth of 64 km, although the Monte Carlo ellipsoid (run with a standard deviation $\sigma_G = 4$ s for the Gaussian noise injected into the dataset) does intersect the Earth's surface. It is nevertheless probable that the earthquake occurred at depth in the Puerto Rico trench as suggested by reports of weak surface waves, and in general agreement with the local patterns of seismicity (Fischer and McCann, 1984). Based on this hypocenter, we have verified that the time given by Collins (1936) as the emergence of the "third group" (04:28:20 GMT) supports its interpretation as a $T$ phase converted to a seismic wave approximately 3°South of the receiver. Subsequent detections of $T$ phases are also reported in the Harvard Bulletin for several Caribbean earthquakes, notably on 18 September and 10 November 1935 (the latter relocating about 40 km West of Montserrat), and 12 December 1936.

Such observations were analyzed in greater detail by Linehan (1940) who only offered speculation as to their nature; in particular, his published illustration of the waveshapes (Fig. 2) appears to be no more than a hand-drawn rendition of their timing. More insightful is Ravet's (1940) contemporaneous but obviously independent report on very short period signals recorded in Tahiti in the wake of distant major earthquakes: the author correctly establishes their association with the epicenter, their generation by the seismic source and their propagation along the surface of the Earth as opposed to through its body. He does estimate a group velocity of 1.5 km/s, but stops short of identifying the latter as the velocity of sound in water, which had been known since the work of Beudant in the Mediterranean Sea in the 1810s and the landmark experiments of Colladon and Sturm (1827) in Lake Geneva.

Indeed, the correct interpretation of $T$ waves as water-borne phases of the seismic source would come only in the wake of the considerable progress in hydroacoustics achieved during World War II, as summarized in a special volume of the Geological Society of America, in which Ewing and Worzel (1948) published the basics of long range propagation in the SOFAR channel, and Pekeris (1948) developed elementary models of the structure of $T$ waves, based on modal theory. These works were complemented by the experimental results of Worzel and Ewing (1948). Simultaneously and independently, Brekhovskikh (1949) published a model for the reverberation of sound in the channel, based on experimental results by Rozenberg (1949).

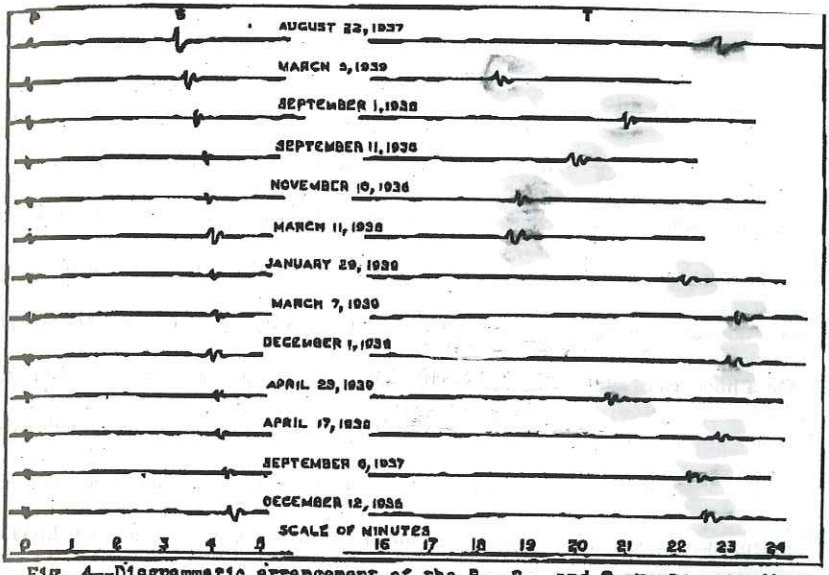


Fig. 4--Diagrammatic arrangement of the P-, S-, and T-groups according to increase in (S-P)-interval

FIG. 2. Reproduction of Linehan's (1940) Fig. 4 (complete with original caption), showing a sketch of $T$ phases from Caribbean earthquakes recorded at Harvard Observatory in the late 1930s. Note that even though the records have been arranged by distance (based on $S - P$ times), the $T$ phases (emphasis added) arrive at irregular times, illustrating the variability of the source-side conversion process; this certainly hindered any simple interpretation of the phase by the author. The diagram was probably hand-drawn, and does not reproduce the waveshape of the $T$ phases; note 10-minute gap in the time scale between the left and right parts of the figure. Adapted from Linehan (1940).

## $T$ Phases as Seismo-Acoustic Conversions

In a number of seminal papers published in the early 1950s, W. Maurice Ewing and his collaborators established the bases of the generation of $T$ phases by earthquakes, as resulting from the conversion of seismic energy to acoustic waves at a source-side solid Earth–liquid ocean interface, followed by the reverse acoustic-to-seismic conversion at the receiver side (Tolstoy and Ewing, 1950). A fundamental aspect of this model is that the existence of sloping interfaces allows the trapping of acoustic energy inside the low-velocity waveguide and hence its efficient propagation to teleseismic distances. In particular, using Caribbean, North and South American earthquakes recorded at Bermuda, Shurbet and Ewing (1957) conclusively modeled their $T$ waves as resulting from conversion of $P$ or $L_g$ phases at an isobath which they selected as 1800 m.

Such models were initially not without detractors, and in particular, Leet (1951) and Leet *et al.* (1951) argued, using occasionally vehemently forceful rhetoric,

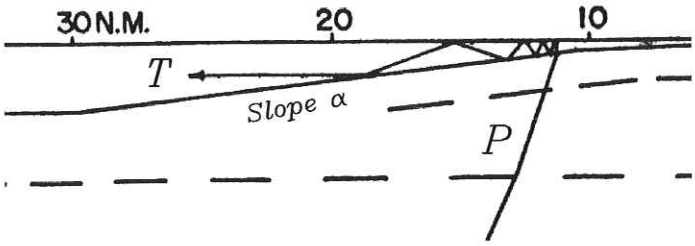


FIG. 3. Principle of the generation of a $T$ phase from an underground source by downslope conversion. The source-side seismic ray (labeled $P$) is converted at the ocean bottom into a steep acoustic ray which is reflected back and forth between the sea surface and the sea floor. In the presence of an interface sloping at an angle $\alpha$, the incidence of the ray is decreased by $2\alpha$ at each bottom reflection, and penetration becomes possible after a handful of reverberations. Adapted (cropped and new labels) from Johnson *et al.* (1963).

that $T$ phases rather represent energy channeled through ocean-bottom sedimentary layers, an idea already expressed by Coulomb and Molard (1949). Later work (e.g., Okal and Talandier, 1981) has indeed documented the possibility of long-range propagation of such waves, but at generally lower frequencies, and with considerable group dispersion (from 0.5 to 2 km/s), not observed in $T$ phases. In their response to Leet's criticism, Ewing *et al.* (1952) correctly pointed out the need for a careful decomposition of the path into its seismic and acoustic portions. When the former become significant, they invalidate any estimate of the velocity of the $T$ phase simply averaged over the entire distance from the source to the receiver.

Despite these early controversies, the work of Ewing and collaborators has withstood the trial of time, in particular concerning the timing of earthquake-generated $T$ waves, which they successfully modeled by summing the contributions of the various seismic and acoustic segments (Shurbet, 1955). In their second paper on $T$ waves in the Lesser Antilles, Coulomb and Molard (1952) reached similar conclusions, but emphasized the importance of $S \rightarrow T$ conversions in specific geometries. At the same time, Wadati and Inouye (1953) underscored the role of steep slopes for efficient conversions, and again of source-side $S \rightarrow T$ conversions notably for moderately deep (70 km) Japanese earthquakes.

In retrospect, it is remarkable that Ewing's group successfully developed their model in the Caribbean-to-New England geometry, which requires complex and long seismic conversions at both ends of the paths. In particular, Fig. 2 (from Linehan (1940)) clearly illustrates the lack of correlation for such paths between the precise timing of $T$ and distance expressed by $S - P$ intervals. By contrast, Ravet (1940) was helped in his interpretation by the generally greater epicentral distances and minimal converted paths at the receiver side in Tahiti.

## The Downslope Conversion Model

Considerable insight was gained throughout the 1960s from the operation, principally by the University of Hawaii, of a wide-aperture network of hydrophone stations throughout the Pacific Basin (Wake, Enewetak, Midway, Oahu, Point Sur). In this framework, Johnson *et al.* (1963) soon developed the concept of "*downslope conversion*" (Fig. 3), originally proposed by Officer (1958). In the presence of a beach sloping at an angle $\alpha$, reverberations of acoustic rays between the seafloor and the ocean surface are deflected by $2\alpha$ at each successive cycle, which eventually allows trapping of the energy inside the SOFAR channel at an angle inclined less than 12° on the horizontal, even though all acoustic rays at the original conversion point would remain much steeper.

The downslope conversion model, based entirely on geometrical optics, proved highly successful at explaining many attributes of the observed $T$ wavetrains. In particular, Johnson *et al.* (1963) modeled lateral changes in the strength and waveshapes of $T$ phases observed at Kaneohe Bay, Oahu from a series of hypocenters in the Andreanof Islands, based on variations in the number of reflections necessary for trapping through downslope conversion. Milne (1959) had used a similar concept to constrain the source of two nuclear tests to the interior of Enewetak lagoon, based on the spectral properties of their teleseismic $T$ waves, which he interpreted as resulting from downslope conversion.

More recently, Talandier and Okal (1998) contrasted $T$ waves received at the French Polynesian Seismic Network (Reseau Sismique Polynésien or RSP), from various types of earthquakes occurring on the Southern part of the Island of Hawaii (Fig. 4). For shallow earthquakes originating near the shoreline, characterized in that area by steep (up to 50°) subaerial and underwater cliffs (the "palis"), the $T$ wavetrains are impulsive, of high amplitude, and feature a fast group time, as a result of a simple conversion process, requiring no more than one reflection to penetrate the SOFAR channel (Fig. 4A). In contrast, for deeper events occurring under the more gentle slopes (typically 15°) of the nearby Loihi volcanic edifice, the $T$ waves are emergent, spindle-shaped, much lower in amplitude, and feature positive delays, as the conversion process requires as many as five back-and-forth reverberations, and is delocalized along the liquid–solid interface (Fig. 4B). In the former geometry, Talandier and Okal (1998) showed that the waveshape of the teleseismic $T$ phase is a simple transposition of the ground motion at the conversion point, as recorded for example by a seismic station in the near field. It is dominated by the $P \rightarrow T$ and $S \rightarrow T$ conversions, the latter featuring a characteristic time delay and a lower frequency content.

Such differences in the efficiency of the conversion process can be transposed to the case of the acoustic-to-seismic conversion at the receiver side, where they can govern the siting of the so-called $T$-phase seismic stations designed to provide high-quality seismic recording of hydroacoustic phases, as mandated under the CTBT (Okal, 2001a). In particular, Okal and Talandier (1998) provided guidelines to define station corrections, in order to account for the receiver-side seismic

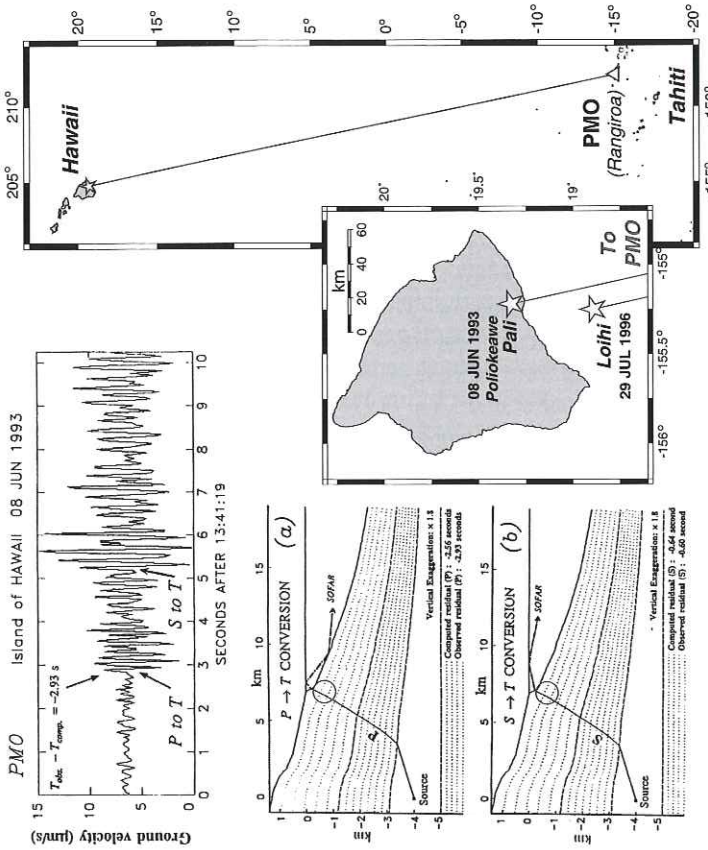
PMO
Island of HAWAII 08 JUN 1993
Ground velocity (μm/s)
SECONDS AFTER 13:41:19
P to T
S to T
Hawaii
PMO
(Rangiroa)
Tahiti
08 JUN 1993
Poliokeawe
Pali
29 JUL 1996
Loihi
To
PMO
km
P → T CONVERSION (a)
S → T CONVERSION (b)
SOFAR
Source
Vertical Exaggeration: × 1.8

FIG. 4A. Comparison of the $T$ waves recorded at Pomariorio (PMO) from two earthquakes on and near the Big Island of Hawaii. *Right*: The maps sketch the general geometry of the focal areas and the path to Polynesia. The 1993 earthquake is located under the steep Poliokeawe "pali" [cliff], while the 1996 event took place deeper and under gentler slopes at Loihi seamount. *Left*: Seismogram of the $T$ phase of the 1993 Pali event at PMO (*Top*) and modeling of the conversion (*Bottom*). Note the impulsive character of the phase, and the clear separation of the $P \rightarrow T$ and $S \rightarrow T$ wave packets. The modeling shows an efficient conversion, requiring only one reverberation, at the steep slope immediately off the shoreline (circles). In this geometry, the $T$ phase is predicted to arrive early relative to acoustic propagation along the whole path, as observed on the record. Adapted (combined; map added) from Talandier and Okal (1998).

path, and showed that $S \rightarrow T$ conversions could become prominent under certain combinations of structure and distance between shore and receiver leading to shadowing for the converted $P$ wave.

## The 1994 Bolivian $T$ Phases

The generation of $T$ phases by intermediate-depth ($70 \leqslant h \leqslant 300$ km) or deep ($h \geqslant 300$ km) earthquakes was mentioned in the very earliest studies by Linehan (1940), Ewing *et al.* (1952) and Shurbet (1955), the latter noticing that a deep focus actually favors $T$-phase generation for large South American earthquakes recorded at Bermuda. We now attribute such observations to the absence of a source-side asthenospheric path otherwise generally responsible for the strong anelastic attenuation, in teleseismic or even regional $S$ waves, of the high-frequency components exclusively capable of penetrating the SOFAR channel.

This remark led to an unexpected development upon the recording (Fig. 5) of spectacular $T$ waves across the entire Pacific Basin following the great 1994 deep Bolivian earthquake (Kirby *et al.*, 1995), an observation itself intriguing given the considerable distance of its 631-km deep source from the oceanic water mass.[†] Okal and Talandier (1997, 1998) further documented that the timing of the Bolivian $T$ waves at receivers across the Pacific required source-side conversion of regional $S$ waves, principally at the Arica Bight. This observation was important from a structural point of view, since the delivery by an $S$ wave, 920 km away from the source, of the high frequencies needed to penetrate the SOFAR (by necessity $f \geqslant 2.5$ Hz; $f \approx 5$ Hz as observed) requires propagation through material with exceptionally low anelastic attenuation. In turn, this implies the continuity of the cold slab throughout the upper mantle, despite the presence of a gap in seismic activity between 300 and 600 km depth in the local Benioff zone, which had led early investigators to propose a broken or detached slab (Isacks and

[†] Indeed, there exists some scant anecdotal evidence that the Bolivian $T$ phase may have been felt on the Southern shore of the "Big" Island of Hawaii (G.J. Fryer, pers. comm., 2000).

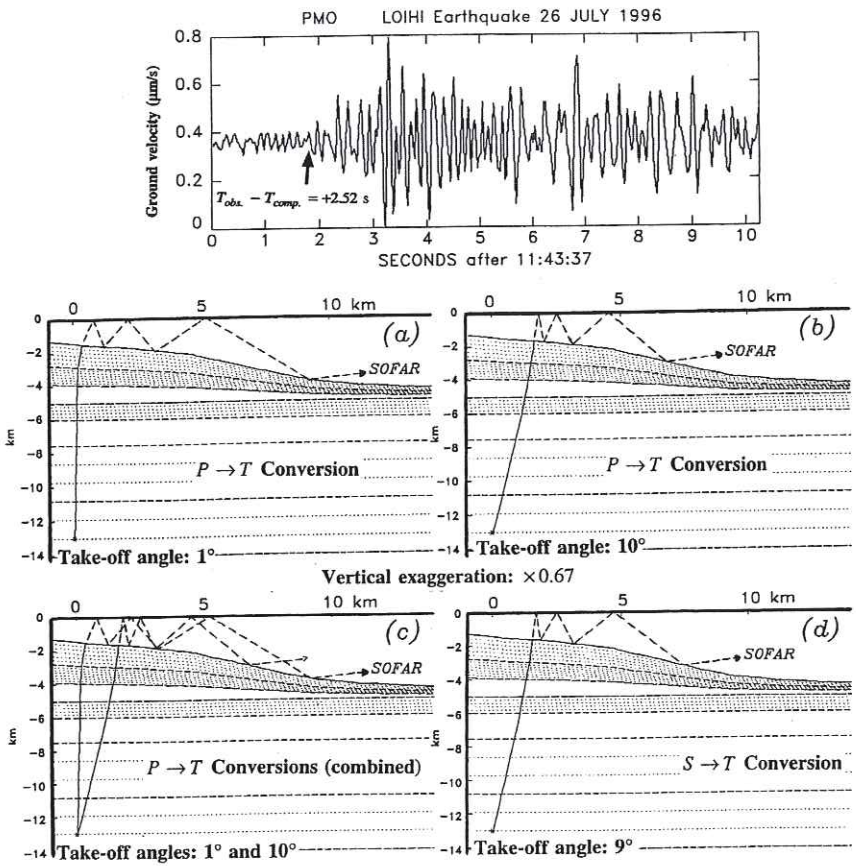


FIG. 4B. Same as Fig. 4A for the 1996 Loihi earthquake. *Top*: $T$ phase record at PMO. Note the emergent phase, with no clear separation of its various components. Also, the phase is significantly late relative to a pure acoustic path from epicenter to receiver. *Bottom*: Modeling of the $P \rightarrow T$ and $S \rightarrow T$ conversions in the presence of a gently sloping beach. In (a) and (b), we show rays departing the focus at 1 and 10° incidence angles. Each requires several reverberations to penetrate the SOFAR channel, and when combined in (c), this results in a wavetrain of longer duration. Frame (d) shows similar characteristics for the $S \rightarrow T$ conversion. Adapted (combined) from Talandier and Okal (1998).

Molnar, 1971). An $S \rightarrow T$ conversion from a deep earthquake then constitutes a proxy for a thermally, and hence mechanically, continuous, low-attenuating slab in the source region, and Okal (2001b) later applied the concept to the so-called "detached" or "outboard" earthquakes, proving in most instances (e.g., Sakhalin, Bonin Islands) that these occurred in warped, rather than detached, segments of the slab. In this framework, $T$ phases can provide an unexpected insight into the deep structural properties of the Earth's mantle.

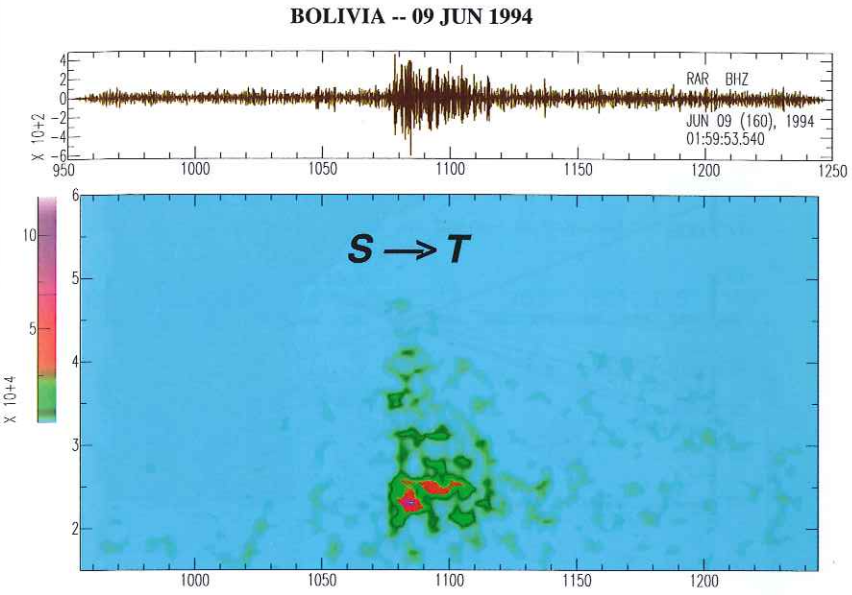


FIG. 5. Examples of $T$ phases generated by deep earthquakes at the bottom of subduction zones. *Left*: Case of the 1994 Bolivian earthquake. The top figure presents a high-pass filtered waveform at Rarotonga and the corresponding spectrogram. Note the presence of a single wave packet, identified by Okal and Talandier (1997, 1998) as an $S \rightarrow T$ conversion at the Arica Bight. The bottom figure shows the geometry of the source side conversion. *Right*: Case of the so-called "detached" 1990 deep earthquake under Sakhalin, recorded at Pomariorio (French Polynesia). Note the presence of two separate wave packets, corresponding to $P \rightarrow T$ and $S \rightarrow T$ conversions, respectively. The presence of the latter requires the continuity of a finger of cold slab, despite the location of the earthquake outboard of the conventional location of the slab. Also, in both instances, note the location of the conversion points at preferential sites along the coast line. Adapted (combined; new material added) from Okal and Talandier (1997) and Okal (2001b).

## Preferential Conversion Sites; On the Road to Scattering

A by-product of Okal's (2001b) investigation was the documentation of preferential sites of source-side conversion, such as the Arica Bight for the deep Bolivian earthquake, and Cape Erimo in Southern Hokkaido, for the Sakhalin one (Fig. 5). This observation was in line with Johnson and Norris' (1968) study of the $T$ waves generated by the 1965 Rat Island aftershock series, which identified loci of preferential conversion for an otherwise largely uniform field of seismic epicenters. Similarly, Walker *et al.* (1992) documented occasional precursors to $T$ phases, attributed to conversion at seamounts neighboring Alaskan and Aleutian epicenters. While observations such as Okal and Talandier's (1997) are still reconcilable with geometrical optics by invoking focusing due to strong

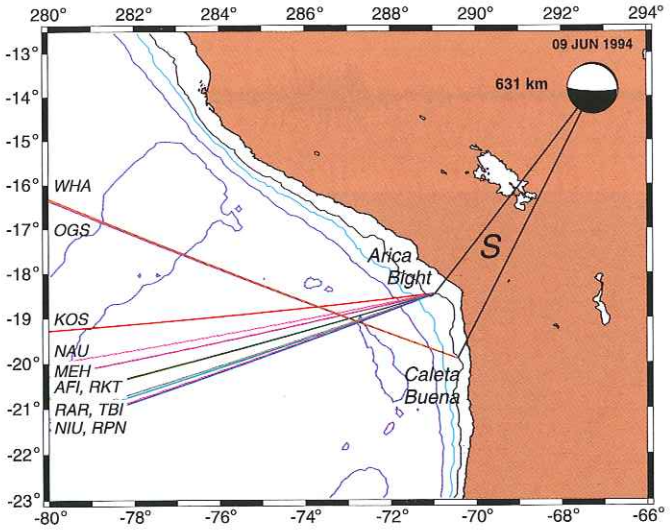


FIG. 5. Continued.

curvature of the mid-SOFAR isobath, Walker *et al.*'s (1992) results suggest the influence of scattering in the generation process.

## The Paradox of the Abyssal $T$ Phase

Furthermore, non-geometrical processes are clearly required to explain the paradox of the so-called "abyssal $T$ phase" sketched on Fig. 6. In this instance, a small intraplate earthquake occurring in a flat abyssal plain, far away from any documented shallow slope, generates a strong $T$ wave throughout the Pacific, whose group times are compatible with generation at the time and epicenter of the seismic source. Note in particular that this property holds not only in the far field (RAR), but also at regional distances (PTCN; 400 km). This indicates that the acoustic wave can be generated in a variety of azimuths in the immediate vicinity of the epicenter, in the absence of a relief appropriate for downslope conversion, and with a minimal, or absent, source-side seismic path. This scenario is reminiscent of Johnson *et al.*'s (1968) observation (Fig. 7) of two components to the $T$ wave of an outer rise Aleutian earthquake ($m_b = 6.3$; 29 July 1965), the relatively impulsive, low-frequency and high-amplitude "downslope" arrival being expectedly late (by $\sim$2 minutes), but preceded by an "abyssal" arrival featuring high frequencies, a low amplitude, and an emergent wavetrain, which appears to originate at the time and location of the seismic source.

In attempting to explain the abyssal $T$ phase, we note that Biot (1952) had initially proposed that a strong coupling could develop between "SOFAR waves" and

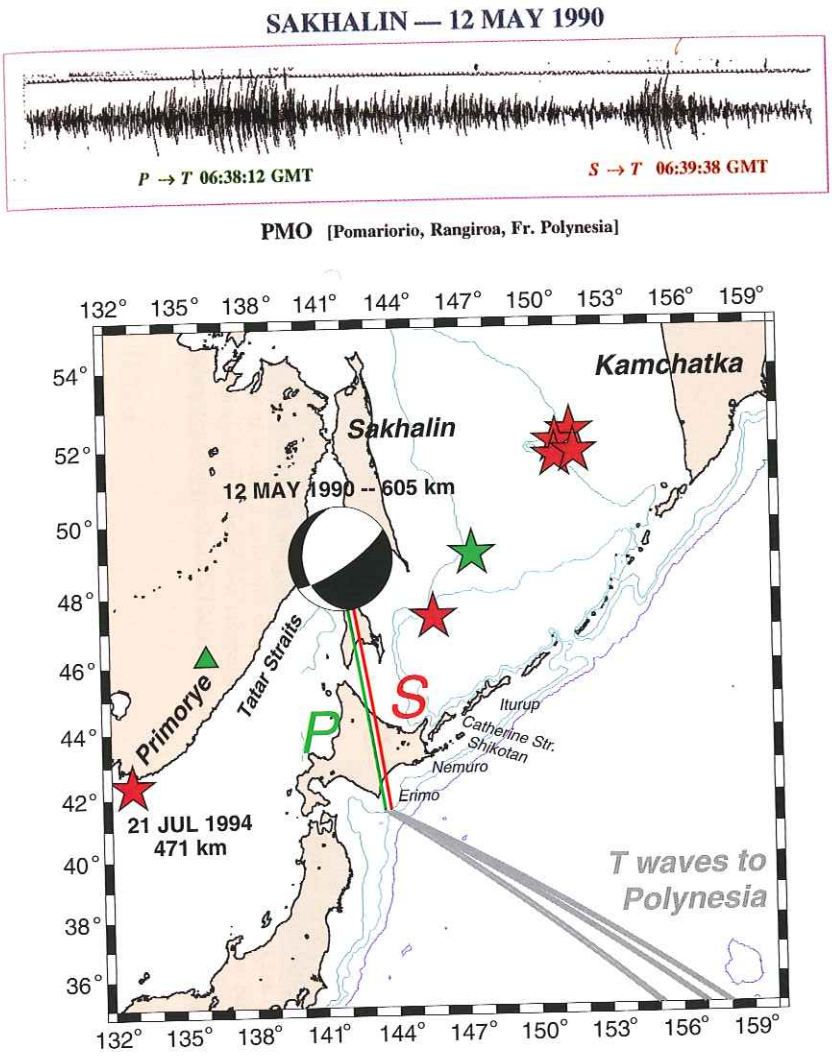


FIG. 5. Continued.

Stoneley waves generated at the solid–liquid interface, which could provide the mechanism for the excitation of an abyssal $T$ phase. However, he did not elaborate beyond the observation that the two systems may have comparable dispersion curves in the high-frequency limit, which may be a necessary but not sufficient condition for the actual development of coupling. This concept was revived recently by the observation by Butler and Lomnitz (2002) of a so-called *Ti* wave, which they define as featuring the propagation characteristics of $T$ phases, while

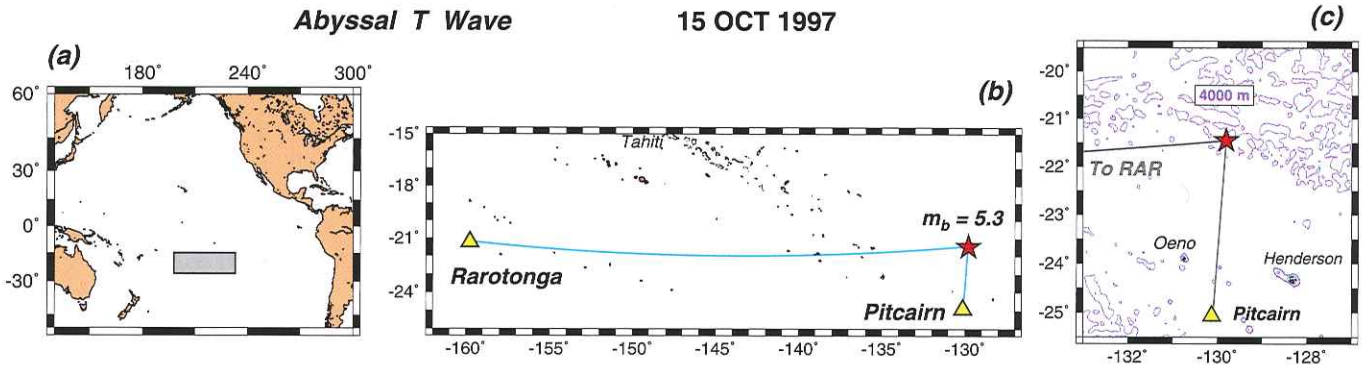


FIG. 6. Example of abyssal $T$ phases generated by a "true" intraplate earthquake, occurring outside any large scale bathymetric feature, (a), (b) and (c): Situation maps of the relevant source and paths. The shaded box in (a) outlines Frame (b). Note the smooth bathymetry of the epicentral area, (d) and (e): Seismograms observed at Rarotonga (RAR) and Pitcairn (PTCN), respectively, high-pass filtered at 1.5 Hz, with relevant spectrograms. Note the long duration (80 s), and emergent character of the $T$ phase, which arrives at a group time in agreement with acoustic propagation along the whole path. The vertical arrows indicate group times calculated from the epicenter for $v = 1.483$ km/s, and in the case of PTCN, the origin time, and *Pn* and *Sn* arrivals. Note that the latter is the dominant phase.

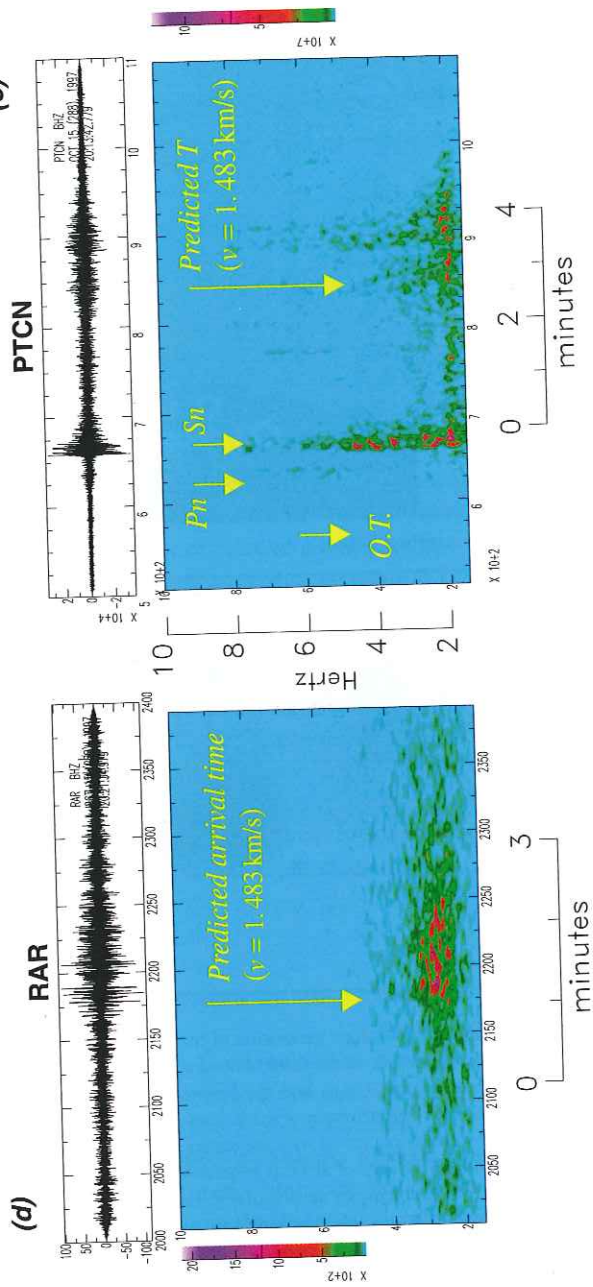


FIG. 6. Continued.

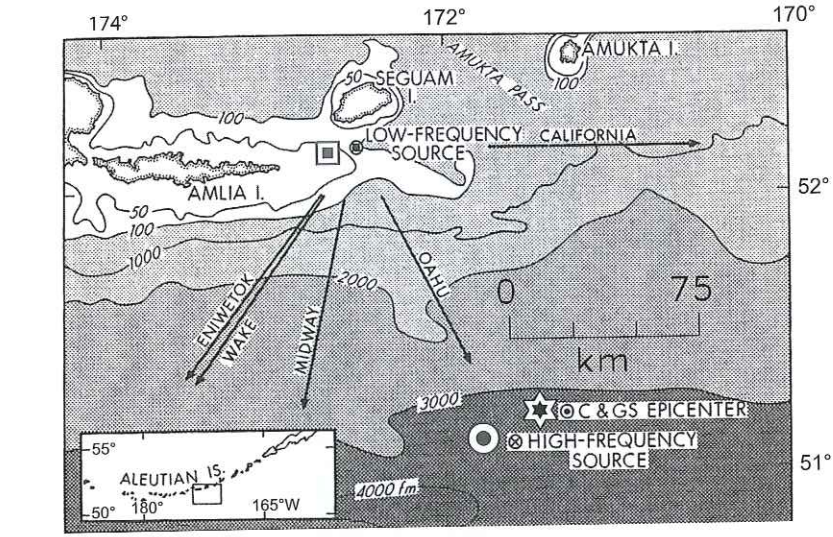


FIG. 7. Combination of abyssal and downslope generation of the $T$ phase for the Aleutian earthquake of 29 July 1965 recorded at Kaneohe, Oahu (after Johnson *et al.*, 1968). *Top*: Map of the source area, showing the epicentral location (star), and the proposed sites of downslope (square) and abyssal (circle) conversions. *Center*: Spectrogram of the $T$ phase contrasting the late, impulsive, high-amplitude and low-frequency downslope arrival with the earlier, emergent, higher-frequency but lower-amplitude abyssal arrival. *Bottom*: Model of abyssal generation as proposed by Johnson *et al.* (1968). The $T$ phase is generated from scattering by an irregular sea surface, in the immediate vicinity of the epicenter, and thus suffers practically no delay, as compared to the downslope-converted phase which first backtracks as a $P$ wave an estimated 150 km. Adapted (combined; cropped; re-labeled) from Johnson *et al.* (1968).

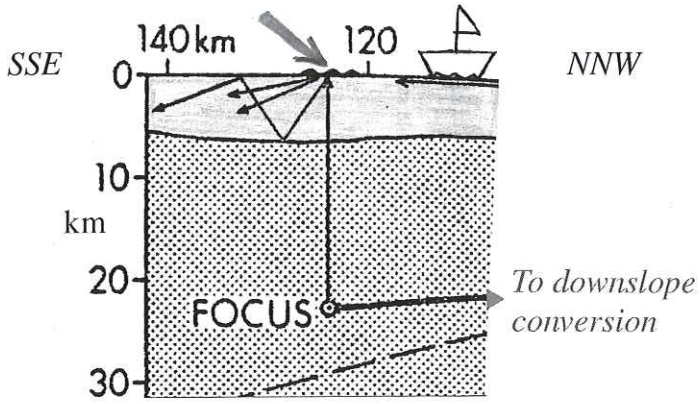


FIG. 7. Continued.

being detected on ocean-bottom or borehole instruments, i.e., in a geometrical shadow for waves guided in the SOFAR channel. However, their model of the propagation of *Ti* in a layer of relatively loose sediments on the ocean floor raises the question of the effect of anelastic attenuation (expected to be high in such structures) on the high frequencies characteristic of the phase.

This leaves a non-geometrical process, such as scattering, as the probable mechanism of generation of the abyssal $T$ phase. Johnson *et al.* (1968) initially attributed its origin to sea surface roughness (Fig. 7), while Keenan and Merriam (1991) later suggested underside scattering by sea ice in the Arctic Ocean, an interpretation obviously limited to polar regions. Later, and most decisively, Fox *et al.* (1994) invoked broad-band scattering by a rough seafloor in the general framework of modal propagation, which forms the basis of the presently consensual interpretation of the abyssal $T$ phase.

## 3. $T$ WAVES IN THE MODE FORMALISM

Modal theory envisions $T$ waves as the superposition of a discrete, albeit in principle infinite, number of *modes* of surface waves guided by the oceanic column, and in particular by the SOFAR channel. The fundamental framework of this approach was developed by Pekeris (1948). Given a flat-layered structure featuring translational symmetry along the horizontal $x$ and $y$ directions, the potential $\phi$ of the elastic wave in the water is sought at each angular frequency $\omega$ as a cylindrical wave radiating out of the polar axis $r = 0$:

$$\phi(r, z, t) = \Phi(z) H_0^{(1)}(kr)\, \mathrm{e}^{-\mathrm{i}\omega t}, \tag{1}$$

where $H_0^{(1)}$ is the Hankel function of first kind and order 0, and $\Phi$ satisfies

$$\frac{d^2\Phi(z)}{dz^2} + \left[\frac{\omega^2}{v^2(z)} - k^2\right]\Phi(z) = 0, \tag{2}$$

$v$ being the local velocity of sound, which can be a priori a function of depth $z$. The boundary conditions, imposing zero pressure at the ocean surface, and zero displacement either at a rigid bottom or as $z \to \infty$, control the existence, at each frequency, of a finite number of *eigenmodes* expressing the relationship between $\omega$ and the wave number $k$, and analogous to the fundamental and overtones of a classical Rayleigh wave.

In his initial study, predating the era of high computational power, Pekeris (1948) first considered the oversimplified model of a single oceanic layer over a *liquid* half-space (Fig. 8a), and explored analytically the properties of the fundamental and first few overtones, closely following Love's (1911) classical analysis of the transverse shear modes of a solid layer over a solid half space. He then extended his investigation to a model featuring two layers over a half space (Fig. 8b), more representative of the SOFAR channel, but still involving exclusively liquids. Pekeris was able to describe the essential dispersive properties of the various branches, in particular the existence of one or several group velocity minima, for various contrasts in sound velocities and layer thicknesses. Most remarkably, he also laid the groundwork for the computation of the excitation of the various modes by an explosive source located in the water, by following Lamb's (1904) classical decomposition of the solution into an integral in the complex wavenumber plane. Such results were remarkably insightful given the simplified representation of the oceanic column as a single layer over a liquid half space, and for that reason, this model, known as a "*Pekeris waveguide*", has remained a benchmark reference for comparisons with modern, much more sophisticated and accurate models of the oceanic column.

Over the next decades, and as detailed for example in Jensen *et al.*'s (1994) comprehensive monograph, improvements in computational techniques, as well as the systematic three-dimensional surveying of the properties of the ocean, have led to more sophisticated models of the structure of guided propagation in the SOFAR channel and of the excitation of acoustic modes by oceanic or land-based sources. Obviously, these developments owed much to the parallel investigation of the theory of seismic waves in layered structures, notably for surface waves by Haskell (1953) (and Harkrider (1964) regarding their excitation by various systems of forces), and for body waves as summarized by Kennett (1983). The following are the milestones most important to our understanding of the excitation and propagation of $T$ waves by earthquake sources.

• *The use of realistic velocity profiles*

Based on a combination of experimental and theoretical work (Tolstoy and Clay, 1966; Pedersen, 1969), Munk (1979) provided an analytical representation

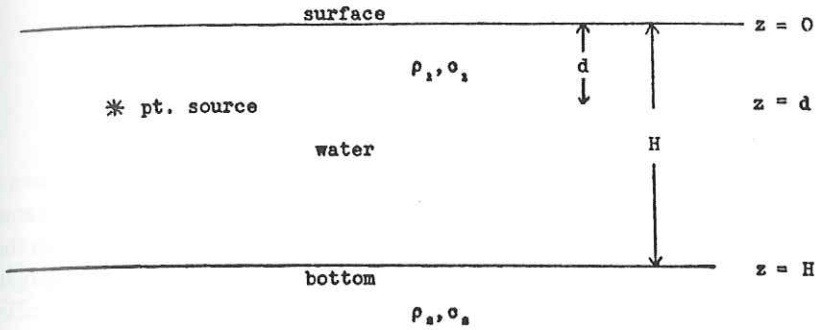


(a) Assumed model for a two-layered liquid half-space

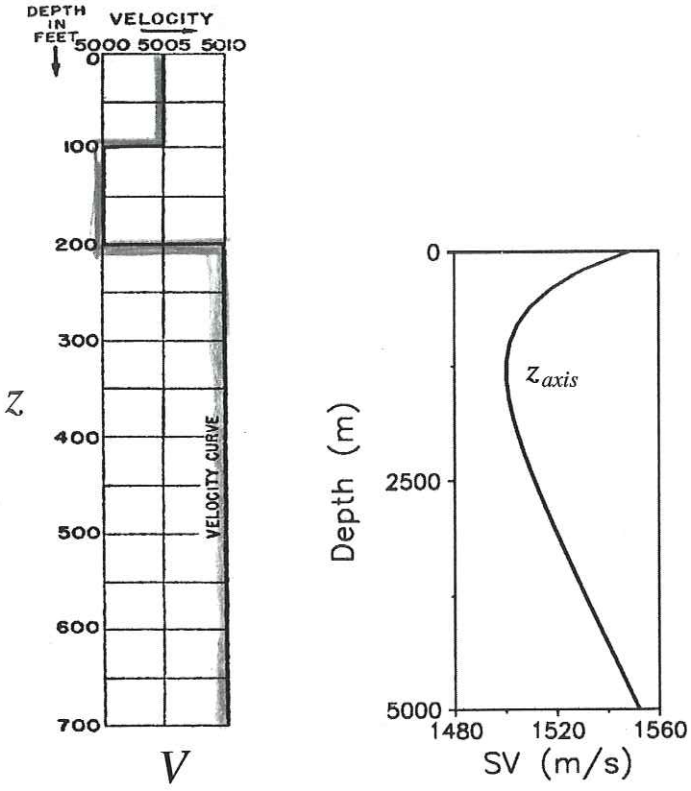


(b) (c)

FIG. 8. Reference models used in theoretical studies of the structure and generation of acoustic modes of the oceanic column. (a): The Pekeris waveguide, consisting of a liquid layer over a liquid half-space; all parameters can be widely varied. (b): Pekeris' later model of a low velocity waveguide, consisting of two layers over a substratum, all media remaining liquid; velocities in ft/s; (c): The Munk sound speed profile described by Eq. (3). Adapted (rescaled; combined; re-labeled) from Pekeris (1948) and Jensen *et al.* (1994).

of a reference velocity profile in the oceanic column,

$$v(z) = v_0\left[1 + \varepsilon\left(\bar{z} - 1 + \mathrm{e}^{-\bar{z}}\right)\right]; \quad \bar{z} = 2\left(\frac{z}{z_{\mathrm{axis}}} - 1\right) \tag{3}$$

where $v_0 = 1500$ m/s, $\varepsilon = 0.00737$, and $z_{\mathrm{axis}} = 1300$ m. This model, known as the Munk profile and shown on Fig. 8c, features a well-developed SOFAR channel centered around the depth $z_{\mathrm{axis}}$. The Sturm–Liouville nature of the problem then allows the use of efficient algorithms (e.g., Wilkinson, 1965) for the systematic computation of literally hundreds of overtones over a wide range of frequencies. The duality between the modal solutions and the optical ray representation can then be investigated in the framework of the WKB approximation (e.g., Ewing *et al.*, 1957; Tindle, 1979). In general, as the mode (overtone) number $n$ is increased at any given frequency, the phase velocity increases, which amounts to steepening the incidence of the equivalent ray.

• *The use of realistic boundary conditions*

The effect of the rigidity of the ocean bottom was addressed early on by Press and Ewing (1950), who considered the case of a single liquid layer over a solid half-space, in particular for an explosive source in the water column. They obtained fundamental results, especially regarding the influence of the finite value of the rigidity of the bottom on the apparent dispersion of the acoustic wave. More systematic investigations of this model (Brekhovskikh and Lysanov, 1982; Jensen *et al.*, 1994) have suggested that the reflection on the solid bottom is well approximated by a Pekeris model in which the sound velocity in the liquid substratum would equal the shear velocity of the solid half-space. This important remark justifies a posteriori the use of the oversimplified Pekeris model.

Figure 9, adapted from Park *et al.* (2001), contrasts, at a single frequency (in this case 5 Hz), the eigenfunction of the first overtone mode (not counting the interface Stoneley mode), with that of a higher ("hybrid") overtone. The former has its energy concentrated around 1000 m depth, in the axis of the SOFAR channel; its properties are equivalent to those described by Pekeris (1948), and in particular, its phase velocity, $C = 1.483$ km/s, expresses propagation of the acoustic energy in the channel. But because its eigenfunction has become essentially negligible by the time it reaches the solid substratum, such a mode cannot be excited by any source in the solid Earth. By contrast, Mode 32 has a well-developed eigenfunction both in the first 12 km of the solid Earth and in the water column; however its phase velocity, $C = 3.438$ km/s, indicates that its energy mostly reverberates at a steep incidence (25°) between the surface and bottom of the ocean, and does not propagate laterally in the SOFAR channel. In this framework, modal theory cannot explain the excitation of an abyssal $T$ phase in a flat-layered structure any better than its geometrical optics dual, namely ray theory.

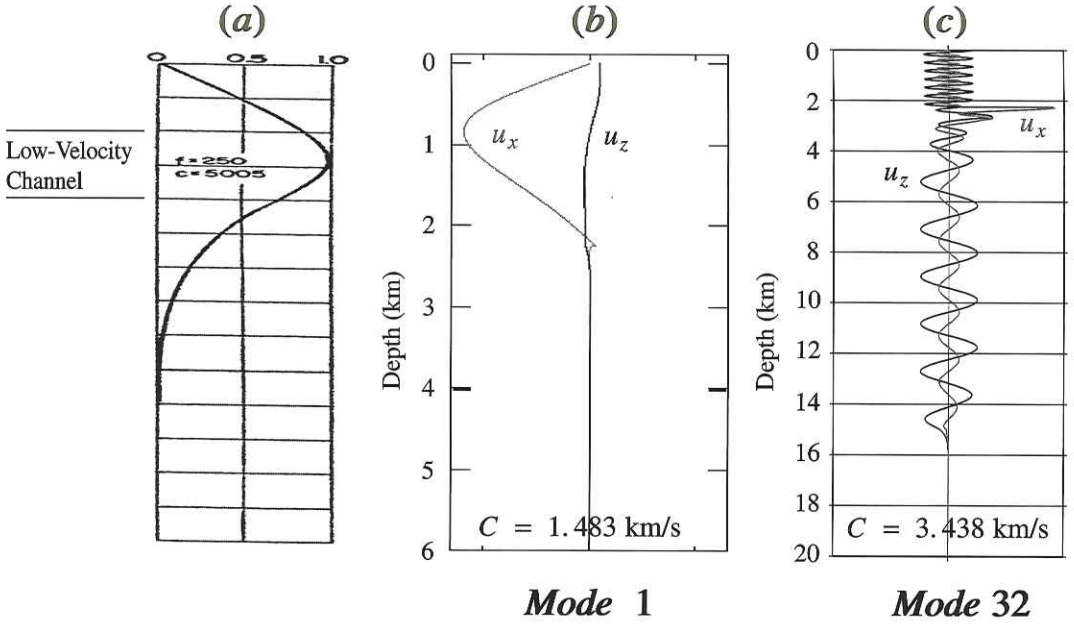


FIG. 9. Theoretical modal solutions reproduced from Pekeris (1948) and Park *et al.* (2001). (a): Pekeris' solution, obtained for his waveguide model shown on Fig. 8b; the plot shows the depth variation of the pressure eigenfunction. (b): First overtone solution at a frequency of 5 Hz, computed by Park et al. for a 2.25-km deep ocean featuring a SOFAR channel; the black line is the eigenfunction of the vertical displacement, the red one that of the horizontal displacement. Note that the mode does not penetrate appreciably the solid Earth. (c): Same as (b) for the 32nd overtone mode, plotted using a different vertical scale. Note that energy is present both in the liquid and solid, but the larger phase velocity expresses the inefficient lateral propagation of the energy in the liquid layer. Adapted (combined; rescaled; re-labeled) from Pekeris (1948) and Park *et al.* (2001).

• *The computation of the excitation of the modes*

At any given frequency, the excitation of the various modes by any source in the ocean column (taken as a point source explosion) or in the solid Earth (taken as an elastic dislocation) is readily computed in the formalisms of Saito (1967) or Gilbert (1970). The summation of the various modes, weighted by their appropriate excitation, allows the synthesis of the wavetrains propagating away from the source, just as the summation of the free oscillations of the Earth excited by an earthquake yields a synthetic seismogram featuring the familiar seismic phases observed at teleseismic distances (Brune, 1964).

• *The application of perturbation theory in the modal framework*

This allows the study of *mode coupling* induced by [weak] lateral heterogeneity of the layered structure under consideration. Most such efforts have considered two types of heterogeneity: one involves two flat basins with different water depths, with a smooth transition extending over several wavelengths, the other a single basin with localized irregularities of the ocean floor, of an amplitude comparable to the acoustic wavelengths (Fig. 10a, b). Based on earlier theoretical work by Shevchenko (1962), Pierce (1965) and Milder (1969), Odom (1986) investigated a number of such scenarios, and in particular, for the second case, derived coupling coefficients between the various modes of the water column. In lay terms, this means that a corrugated structure of the type shown on Fig. 10b can provide a mechanism to leak energy from modes with little if any amplitude in the SOFAR channel (but strongly excited by underwater earthquake sources) into modes representing propagation of energy trapped into the channel (but not excitable by underground sources). This approach provides the key to a satisfactory explanation of the generation of the abyssal $T$ phase by scattering at the ocean bottom.

More recently, Park and Odom (1999) extended the concept to the case of a stochastic field of heterogeneities on the seafloor, and Park *et al.* (2001) applied their results to a number of scenarios involving different geometries and depths of earthquakes under both a homogeneous ocean–bottom interface, and a heterogeneous one, which could be deterministic (as in the case of the sloping interface) or stochastic (i.e., featuring random roughness). Figure 10c (adapted from Park *et al.* (2001) quantifies, for a flat-layered structure and at $f = 5$ Hz, the seismic amplitude excited into the various overtone branches, and illustrates that only those modes with overtone numbers $n = 18$–$55$ are significantly excited. Figure 10d similarly shows the kernels for conversion of the elastic field in (c) by various scatterers located at the ocean bottom. Once multiplied by a scattering function expressing the density of heterogeneity in models such as (a) or (b), the kernels yield the cross-over amplitudes converted into the various modes. Note that the horizontally propagating water modes ($n = 1$–$10$) are now excited with a finite amplitude; this expresses the key result of the model, namely that it can indeed predict the excitation of an abyssal $T$ phase.

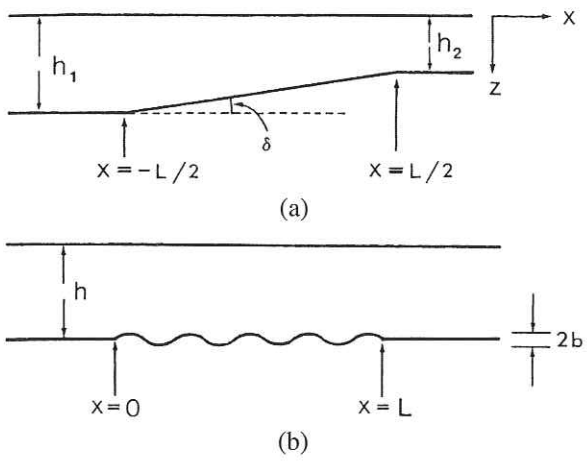


FIG. 10. (a) Example of lateral perturbation of a flat-layered ocean model: Two basins of depths $h_1$ and $h_2$ are connected by a slope. (b): Model of a corrugated segment of ocean floor in an otherwise laterally homogeneous flat-layered structure. (c): Initial excitation, at $f = 5$ Hz, of the various overtone modes of a flat-layered structure by a double-couple source located at 9 km depth (the ocean layer, 2.25 km deep, is shown in darker tone). Note that only overtones of order 18–55 are substantially excited. In particular the lower overtones corresponding to propagation in the water column are not. (d): Mode excitation by sea-bottom scattering. Note that the energy of the higher modes in (c) has been converted into the lower overtones (of order less than 10), propagating in the SOFAR channel. See text for details. Adapted (combined; re-labeled) from Odom (1986) and Park *et al.* (2001).

Park *et al.* (2001) further documented that relatively deep earthquakes ($h =$ 80 km) can excite $T$ waves through scattering by a rough ocean bottom, and also proposed that strike–slip earthquakes seem especially efficient at generating $T$ phases, as observed by Dziak (2001), and further discussed below.

Finally, Odom and Soukup (2004) examined the amplification of the scattering process in the presence of an intermediate layer of low-rigidity sediments, which can be regarded as the mode dual of the well-known amplification of strong motion by sedimentary structures routinely observed in classical seismology (e.g., Gutenberg, 1957; Bard *et al.*, 1988).

Following a different strategy, Schmidt *et al.* (2004) model the scattering of acoustic energy into the water column through the Virtual Source Approach, which uses the Rayleigh–Kirchhoff approximation. They show that abyssal $T$ phases can be interpreted as resulting from scattering of seismic energy trapped in sedimentary layers in the form of Scholte waves (Scholte, 1947).

Using a simplified methodology, deGroot-Hedlin and Orcutt (1999) modeled scattering into a given acoustic mode by sea-floor heterogeneities as directly proportional to the product of the amplitude of the mode at the ocean–sediment interface and of the ground motion produced by the dislocation source at the relevant location. They emphasize that the bottom modal amplitude is strongly

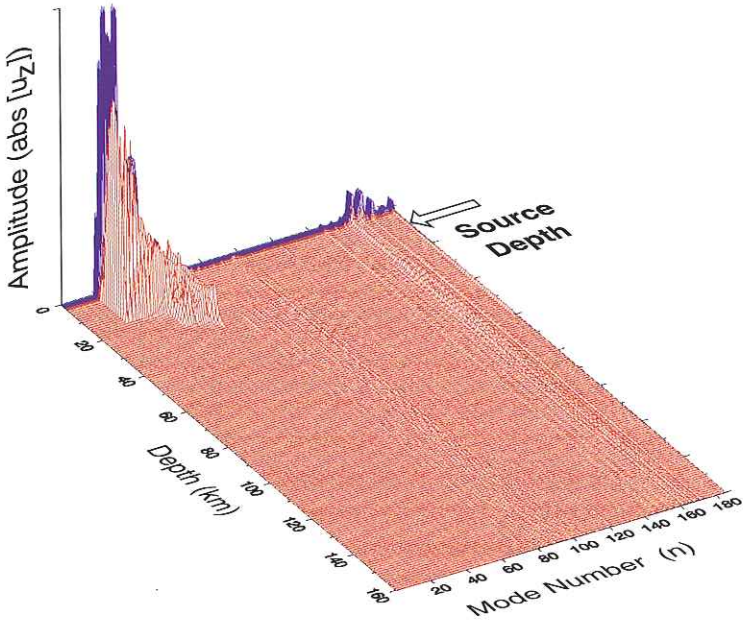


(c)

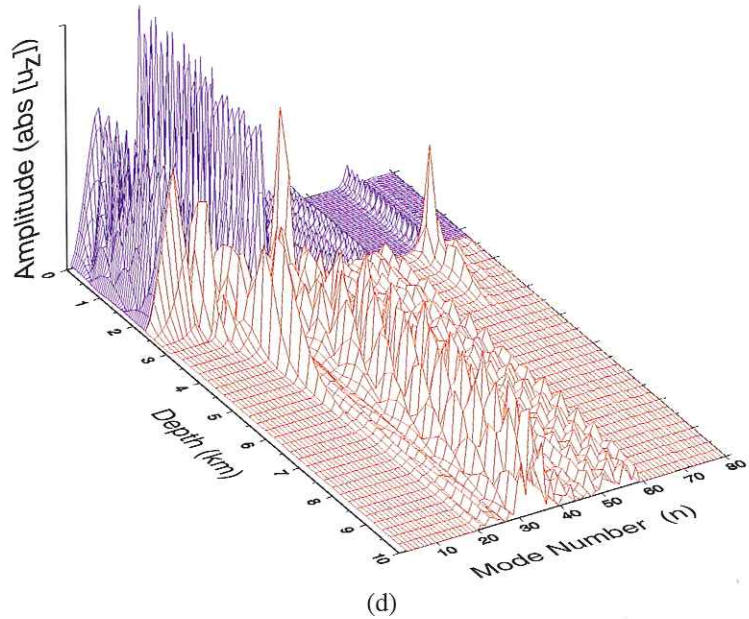


(d)

FIG. 10. Continued.

dependent upon the depth of the water column (mostly decreasing with increasing depth below a few hundred meters), and that the scattering process generating the $T$ phase is thus strongly controlled by bathymetry. When combined with differences in propagation times for $T$ waves generated at various locations on the ocean floor, this model successfully explains differences in the shape of envelopes observed at Wake Island for $T$ phases originating at various subduction zones of the Northern Pacific (Fig. 11).

Yang and Forsyth (2003) later expanded on deGroot-Hedlin and Orcutt's (1999) model by including the contribution of $S$ waves to the ground motion at the conversion point, and by assigning only a small fraction (typically 1%) of the incident amplitude to scattering in a horizontal direction; however, they also consider the effect of scattering when reverberating rays traveling quasi-vertically in the water column hit the ocean bottom at later times, thus contributing to the extended duration of the $T$ phases. As shown on Fig. 12, this approach allowed Yang and Forsyth (2003) to produce very realistic renditions of the envelopes of abyssal $T$ phases recorded at regional distances by an array of ocean-bottom seismometers, and in turn to improve on the definition of group times for such signals, and eventually on the precision of location algorithms using $T$ phases.

## 4. Using $T$ Phases to Detect and Locate Seismic Sources

Since $T$ phases can transmit energy from small sources over large distances, they provide an exceptional opportunity to detect and locate small seismic events which would otherwise have gone unsuspected. In this context, $T$ phases have been used primarily to refine our knowledge of the low-level seismicity of mid-oceanic ridge systems and of intraplate abyssal basins.

As a result of the operation by the University of Hawaii of a wide aperture hydrophone array in the Pacific, Duennebier and Johnson (1967) located more than 20,000 $T$-phase sources in the Pacific Basin in 1964–1967, and compared them with the dataset of USCGS epicenters for the same period (numbering roughly half as many events). The authors identified regional trends in spaciotemporal differences between solutions derived from $T$ phases and conventional seismic waves, which could often be ascribed to the influence of source-side processes such as downslope conversion. They presented maps of the Pacific Basin divided in quadrangles where they compared seismicity defined by seismic and $T$ phases, which suggest that the latter reveal many more events at mid-oceanic ridges and occasionally in abyssal plains; Walker (1989) later included 206 such epicenters in a catalog of intraplate seismic events.

Using the same database, Northrop *et al.* (1968) focused on the Juan de Fuca and Gorda Ridge systems where they described earthquake epicenters in the framework of small scale ridge-and-transform segments. Later, Hammond and

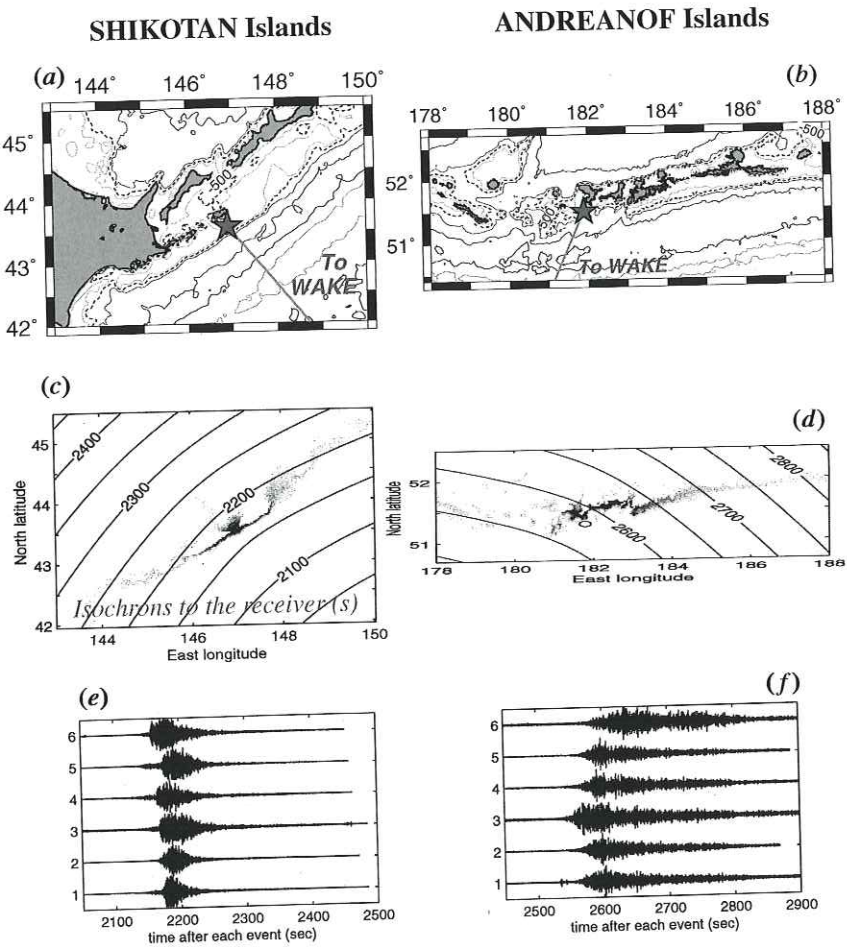


FIG. 11. Modeling of $T$-wave generation by scattering at continental or island arc slope, after deGroot-Hedlin and Orcutt (1999). The authors contrast the case of $T$ phases received at the Wake Island hydrophone from earthquakes in the Shikotan (a) and Andreanof (b) Islands. In (c) and (d), they map the intensity of the scattered $T$ phase on the ocean floor as a function of the seismic amplitude reaching the epicenter and of the excitation of acoustic modes (essentially mode 1) at the relevant depth. The contours represent isochrons to the receiving station at Wake. The aspect ratio of frame (d) has been corrected to make the map conformal and give it the same scale as the Mercator projection in (b). Synthetic waveforms are presented in frames (e) and (f) by summing up the contributions of the various scatterers. Note the greater geometrical scatter of the secondary sources in the Andreanof case, which combines with the different orientation of the path to Wake to give the signal a greater dispersion in time, and hence a more spindled shape. Adapted (combined; rescaled; maps added) from deGroot-Hedlin and Orcutt (1999).

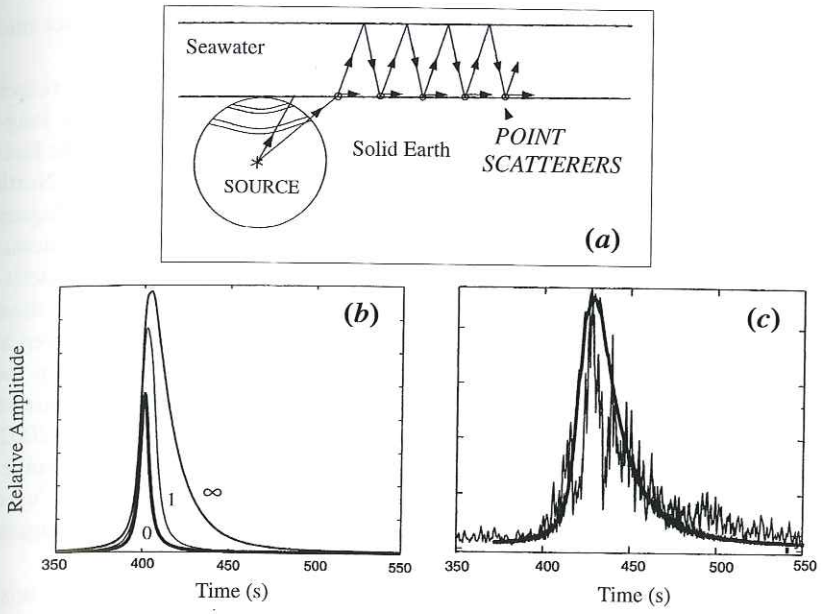


FIG. 12. Generation of the abyssal $T$ phase by a field of scatterers on the ocean floor, after Yang and Forsyth (2003). (a): General layout of the concept: the ocean floor is illuminated both directly by the seismic source, and through reverberation of steep acoustic rays in the water column. At each reflection or transmission point, a small fraction (1%) of the elastic energy is scattered in a horizontal direction, and thus made available for penetration of the SOFAR channel. (b) $T$-phase envelopes synthetized from scattering by the $P$-wave near field of a symmetric (explosive) source. The thick line (labeled "0") is the direct field including no reverberation, the intermediate one (labeled "1") includes the effect of a single reverberation and the outer curve (labeled "$\infty$") includes a very large number of reverberations. (c): Comparison of a $T$-wave envelope synthetized using the geometry of the full field of a strike–slip dislocation (including $S$ waves; thick line), and of an observed waveshape; note the generally good agreement of the waveshapes. Adapted (combined; rescaled; re-labeled) from Yang and Forsyth (2003).

Walker (1991) located 54 otherwise undetected earthquakes (as well as 4 reported ones) on the Juan de Fuca and Endeavor Ridges, which they attributed to volcanic activity during episodes of sea-floor spreading.

The partial declassification of the Sound Surveillance System (SOSUS) network of U.S. Navy hydrophones in 1991 resulted in much enhanced location capabilities in the Northeast Pacific, which allowed Fox *et al.* (1995) to closely monitor, in real time, the spatial evolution of a swarm of more than 600 earthquakes on the Juan de Fuca Ridge, starting on 26 June 1993. This was interpreted as part of a lateral dike injection by Dziak *et al.* (1995), and resulted in the "rapid response" dispatch of a multidisciplinary team of investigators for what turned out

to be the first in situ observation of volcanic activity on a segment of mid-oceanic ridge (Embley *et al.*, 1995).

Following these developments, systematic monitoring of mid-oceanic ridges was instigated through the deployment, illustrated on Fig. 13, of two long-term, wide aperture so-called "autonomous" hydrophone arrays, around the fast-spreading Equatorial Pacific Rise (Fox *et al.*, 2001) and the slow-spreading North Atlantic Ridge (Smith *et al.*, 2002). By providing extremely detailed catalogues of the spaciotemporal distribution of seismicity on and around the ridge systems, these still ongoing projects have shed considerable new light on the characteristics of ridge earthquakes, both of tectonic and volcanic origin. Among the most important results is the confirmation of the generally aseismic character, even at low source levels, of fast-spreading segments, with all tectonic activity on the EPR located on the transform faults (Fox *et al.*, 2001), in contrast to the case of slow-spreading ridges (Smith *et al.*, 2003). In addition, Bohnenstiehl *et al.* (2002, 2003) provided very detailed imaging of aftershock sequences in several geometries, and documented high values, in the median valleys, for the parameter $p$ used to fit the Modified Omori Law to temporal distributions of aftershocks (Ogata, 1983), which these authors attributed to a local field of high temperatures.

Using an independent approach, Forsyth *et al.* (2003) combined near-field seismic and $T$ phases recorded by an array of ocean bottom seismometers to precisely locate a swarm of activity along the Equatorial East Pacific Rise system, and documented coupling between nearby short transform fault segments; they tentatively interpreted the swarm as the only manifestation of an otherwise silent episode of "aseismic" slip comparable to creep events detected on the San Andreas system (Linde *et al.*, 1996).

On a teleseismic, basin-wide scale, it is expected that deployments such as the autonomous Equatorial Pacific Hydrophone Array (EPHA) will lead to a better definition of the level of seismicity of abyssal basins. However, systematic tests performed by Fox *et al.* (2001) showed that precision and accuracy in epicentral range (as opposed to azimuth) quickly deteriorate when the source moves far outside the recording array. Figure 14 (adapted from Fox *et al.*, 2001) clearly illustrates this smearing of epicentral location on great circles radiating from the array, but would still suggest, over and beyond this effect and the possible influence of acoustic blockage to certain provinces, recognizable patterns of variability in the intraplate activity of the Pacific Basin. For example, the relatively large level of activity inside the Nazca plate (at distances not exceeding 1.5 times the maximum dimension of the array) would agree with the conclusions of Wysession *et al.* (1991).

On the other hand, it is clear that the location capabilities of the EPHA could be drastically improved by the addition of a single hydroacoustic receiver such as the CTBT hydrophones at Juan Fernandez, or $T$-phase stations such as those of the Polynesian Seismic Network (Fig. 14). Also, the synergetic use of acoustic and seismic phases should significantly improve location capabilities of small

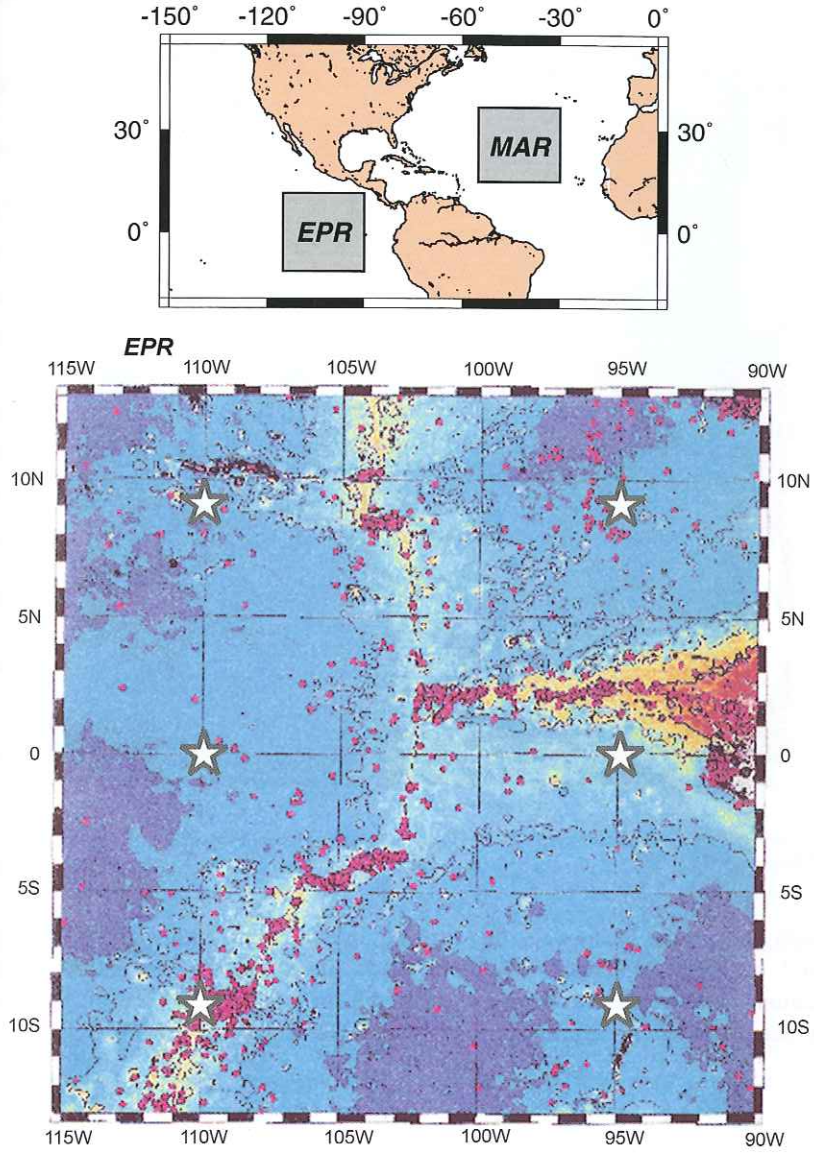


FIG. 13. Regional epicenters located by the autonomous arrays of hydrophones (large stars) recently deployed around the Equatorial East Pacific Rise (EPR) and the Northern Mid-Atlantic Ridge (MAR). The bottom maps contrast the seismicity patterns along the slow-spreading MAR, where earthquakes are ubiquitous along both transform and spreading segments, and along the fast-spreading EPR, where the latter are essentially silent, except for occasional events presumably associated with magmatic swarms at axial volcanoes. Adapted (combined; enhanced; map added) from Fox *et al.* (2001) and Bohnenstiehl *et al.* (2003).

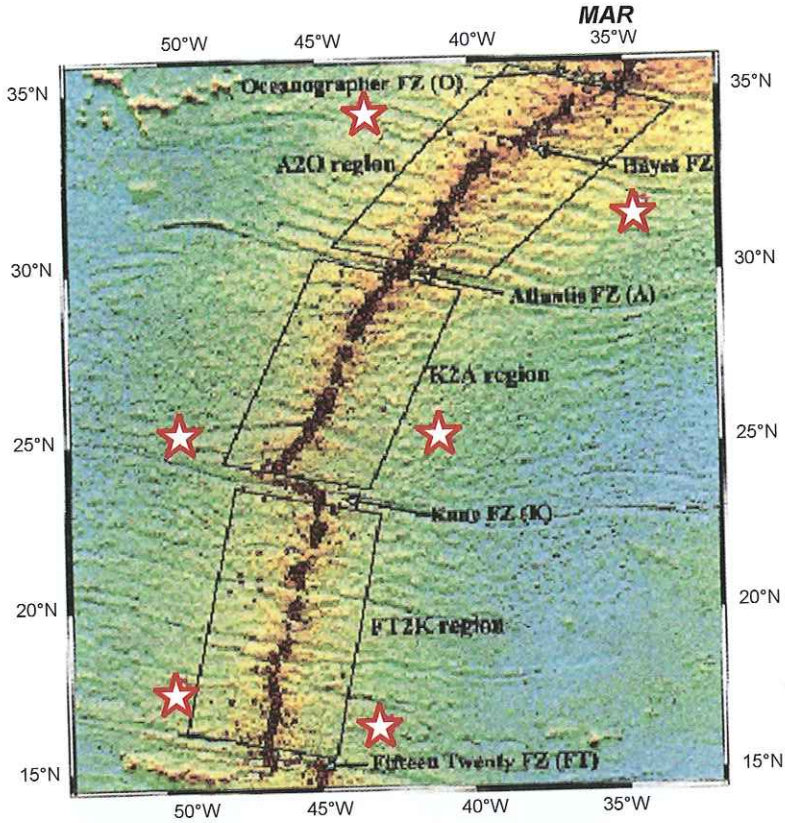


FIG. 13. Continued.

events even in the far field. In this respect, Talandier and Okal (2004b) showed that $T$ waves could be used to compensate for the systematic bias introduced in locations of underwater explosions achieved from ground-based seismic stations, and due to the lateral heterogeneity of crustal phases at continental margins.

## 5. USING $T$ WAVES TO EXPLORE THE SEISMIC SOURCE

We discuss in this section several approaches to extracting from a $T$-phase waveform quantitative information relative to the earthquake source. Despite the complexity of their generation process, $T$ waves are but one of the numerous seismic phases generated by an elastic dislocation. As such, they should carry information about earthquake source spectra in the high-frequency range

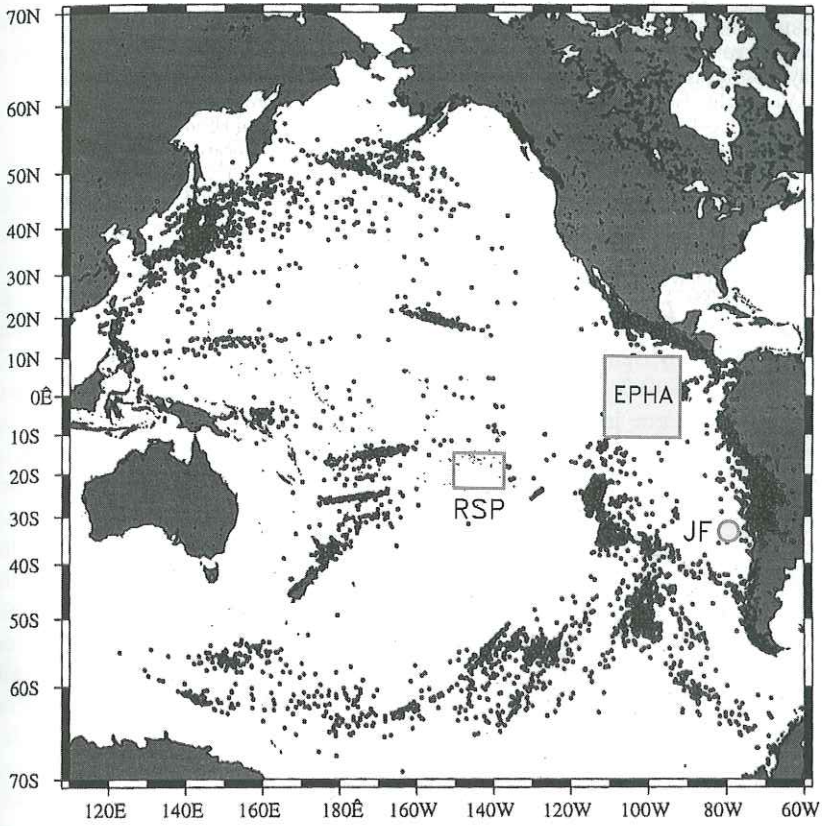


FIG. 14. Far-field epicenters located by Fox *et al.* (2001) from detections at the Equatorial Pacific Hydrophone Array (EPHA). The extent of the array is shown by the shaded box. Note the streaks of epicenters along great circles radiating from the array, which express the loss of range resolution for very distant events. The location of the new hydrophone station at Juan Fernandez Island (JF) is shown by the large circle and that of the Polynesian Seismic Network (RSP) by the open box. Adapted (re-labeled) from Fox *et al.* (2001).

($f \geqslant 2.5$ Hz), otherwise poorly sampled due to anelastic attenuation of conventional teleseismic waves. However and as detailed below, for larger earthquakes, $T$ waves are strongly affected by interference resulting from source finiteness, and their amplitude alone cannot be a good proxy for source size. For this reason, the independent measurement of $T$-wave *duration* is necessary to retrieve an adequate estimate of an earthquake's size. We discuss below the joint use of amplitude and duration, which can take two forms: by combining their values, in the form of the $T$-Phase Energy Flux (TPEF), Okal *et al.* (2003) extended to $T$ waves the concept of radiated seismic energy applied to body waves by Boatwright and Choy (1986); by contrasting them in the form of an amplitude-duration criterion,

Talandier and Okal (2001) allowed the discrimination of explosive and dislocative sources, and more generally the identification of unusual seismic sources, such as slow earthquakes and possibly landslides.

## Background: Source Finiteness for $T$ Waves

While early investigators sought an interpretation of $T$-wave amplitudes in terms of earthquake magnitudes, the high-frequency nature of the $T$ phase makes it particularly vulnerable to destructive interference due to source finiteness which leads, for large sources, to the eventual saturation of spectral amplitudes measured at any fixed frequency. This concept was introduced in the case of conventional seismic waves by Ben-Menahem (1961) and studied in detail by Geller (1976) in his seminal paper on the saturation of magnitude scales. Essentially, the growth of a seismic source in a material with given ("invariant") elastic properties requires extending the source both in time and space. Any measurement taken on a seismic wave at a given frequency $f$ will suffer from destructive interference as soon as its period $1/f$ (or wavelength $\Lambda$) becomes comparable to, or shorter than, the duration (or spatial extent) of the source. The combined effect of the finite strain release on a 2-dimensional fault and of the limited velocity of the actual slip between the fault walls leads to a total saturation of spectral amplitudes once the source corner frequencies recess below the frequency $f$ of interest in the wave group under study. On this basis, Geller (1976) justifies the well-known saturation of the 20 s surface-wave magnitude $M_s$ around 8.2 for moments $M_0 \geqslant 10^{28}$ dyn cm, and similarly of the body-wave magnitude $m_b$ around 6.3 ($M_0 \geqslant 1.8 \times 10^{26}$ dyn cm) when properly measured on $P$ waves at 1 second (larger values of $m_b$ reported in bulletins usually stem from measurements taken at longer periods, or on $S$ waves, or relate to deep events allowing greater strain release). The destructive nature of the interference will be exacerbated for $T$ waves, which are limited to $f \geqslant 2.5$ Hz by the geometry of the SOFAR channel, and saturation would be expected to take place as early as $M_0 > 2 \times 10^{25}$ dyn cm (equivalent to $m_b = 6.0$ or $M_s \geqslant 6.4$) (Geller, 1976; Talandier and Okal, 1979). Note also that the use of source scaling laws assumes the invariance of the seismic-to-acoustic processes, which can be a gross oversimplification, given their complexity and their variability for any population of sources (e.g., Johnson *et al.*, 1963, 1968).

In this general framework, we review early results on the quantification of $T$ waves, as well as more recent and promising developments.

## Amplitude Measurements

An early attempt at relating $T$-phase amplitudes to earthquake magnitudes is found in Johnson and Northrop (1966), who studied 49 records from Aleutian earthquakes. They quantified $T$ phases through their so-called *strength* (*TS*), expressed in dB over a reference pressure of 0.1 μbar, and proposed a relation of the

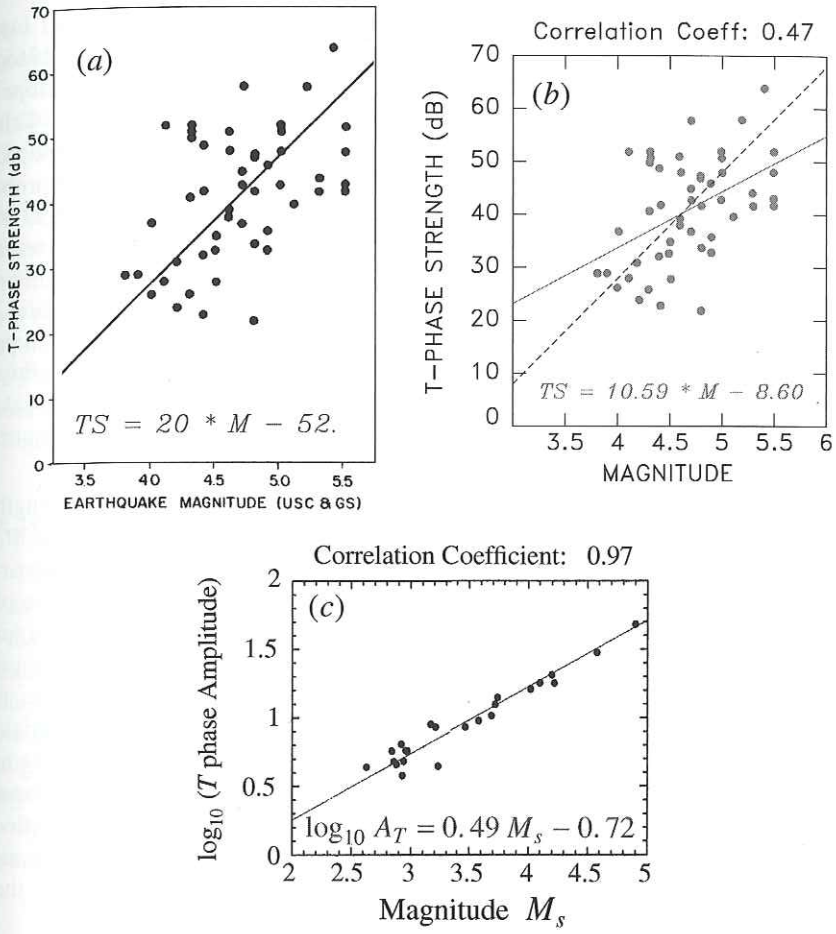


FIG. 15. Examples of correlation between earthquake magnitude and $T$-phase amplitudes. (a): Correlation with $T$-phase strength after Johnson and Northrop (1966). In (b), the same dataset is fit by least-squares. Note the mediocre correlation coefficient, and the much reduced slope, when the latter is left to float; the dashed line reproduces the regression proposed in (a). (c): Correlation with surface-wave magnitude for 24 East Pacific Rise earthquakes (Yang and Forsyth, 2003). This diagram has been replotted using the exact the same orientation and scales as in (a) and (b). Note the much improved correlation. Combination (re-labeled, rotated, combined) of new material (b) and material (a) from Johnson and Northrop (1966), and (c) from Yang and Forsyth (2003).

form

$$TS = 20M - 52 \quad \text{(Fig. 15a)}. \tag{4}$$

However, this approach has several shortcomings. First, the constant 20 was fixed, under the assumption that the $T$-phase amplitude should parallel seismic

amplitude; second, it is not clear which magnitude ($m_b$; $M_s$) is used in (4). We conducted an independent regression of Johnson and Northrop's (1966) dataset allowing the slope to float (Fig. 15b), which yields a much gentler slope: $TS = 10.59M - 8.60$, but a mediocre correlation coefficient of only 0.47. This lower value of the best-fitting slope indicates that $T$-phase amplitudes are indeed affected by destructive interference in a range of magnitudes where $M_s$ (and probably $m_b$) should not be. Fox *et al.* (2001) also reported a lower value ($7.84 \pm 2.04$) of the slope of acoustic source level (in dB) vs. $m_b$ for a dataset of 87 events recorded at the Autonomous Equatorial Array. Such results are also in agreement with those of Yang and Forsyth (2003), reproduced on Fig. 15c, who regress the amplitude $A_T$ of $T$ phases as $\log_{10} A_T = 0.49M_s - 0.72$ (equivalent to a slope of 9.8 between $TS$ and $M_s$ in (4)) for a very homogeneous dataset of 24 East Pacific Rise earthquakes at regional distances. The factor 0.49 similarly expresses that $T$-wave amplitudes do suffer from interference effects in a range of magnitudes ($M_s \leqslant 5$) where 20-second waves are immune from them.

Walker *et al.* (1992) later investigated the correlation of $T$-phase strength (which they restricted to the frequency range 10–35 Hz) with seismic moment $M_0$ for a dataset of 25 Pacific-rim earthquakes recorded at the Wake hydrophone array. The use of $M_0$ should ensure a more robust estimation of the true size of large events, and Walker *et al.* (1992) indeed observe an excellent correlation for certain sub-datasets (their Fig. 17), but their results are difficult to interpret since most of their large moments involve strike–slip sources in the Gulf of Alaska; as discussed below, this geometry may be a preferential $T$-phase generator (Dziak, 2001), and those strike–slip earthquakes may thus not be directly comparable to the remainder of the dataset, consisting almost exclusively of thrust and normal events. Hiyoshi *et al.* (1992) similarly studied 17 Japanese earthquakes recorded at Wake. They observe a strong correlation between $TS$ and $\log_{10} M_0$, but the resulting slopes are only half of those suggested by Walker *et al.* (1992), and the earthquakes in their dataset are generally smaller.

## Duration: Another Measure of Source Size

As source size is increased, so is the time it takes for the rupture to take place at any given point on the fault, and more significantly to propagate along the full extent of the fault zone. As a result, scaling laws predict that the duration of any seismic wavetrain should also grow, in principle linearly with the dimension of the source, or like $M_0^{1/3}$. This idea forms the basis of the use of duration magnitudes (e.g., Lee *et al.*, 1972; Real and Teng, 1973), and it would be expected that the duration of $T$ waves should also grow with source size.

Indeed, a number of early studies sought to measure the duration of the $T$ phase of large shocks in relation to their size. Eaton *et al.* (1961) noted that the $T$ phase of the 1960 Chilean earthquake lasted as much as 6 minutes, while Ben-Menahem

and Toksöz (1963) proposed 4 minutes for the 1958 Fairweather, Alaska earthquake. However, neither of these authors gave a formal definition of duration. Following an idea suggested by Johnson (1970), Okal and Talandier (1986) analyzed a large dataset of $T$ waves from Pacific shocks recorded in Tahiti and Hawaii, and obtained reasonable correlations between their durations and various magnitude scales. They defined the duration of the wavetrain either as that of sustained maximum amplitude, or that of saturation on paper records at Polynesian stations. In particular, they showed that $T$-wave duration keeps growing with seismic moment, even for the very largest seismic events (Alaska, 1964; Chile, 1960). Consequently, Okal and Talandier (1986) suggested the use of $T$-phase duration as an indicator of the tsunamigenic potential of large earthquakes, with a threshold of 100 s for the excitation of a destructive transoceanic tsunami ($M_0 \geqslant 5 \times 10^{28}$ dyn cm). They noted, however, the presence of outliers in their dataset, notably strike–slip earthquakes on the Alaskan Fairweather Fault.

### $T$-Phase Energy Flux: The Parameter $\gamma$

In an attempt to characterize the total energy generated by an earthquake source into a $T$ wave, Okal *et al.* (2003) introduced the concept of the *$T$-Phase Energy Flux* (TPEF), which mimics the estimated energy $E^E$ developed by Newman and Okal (1998) for body waves. The latter was itself inspired by Boatwright and Choy's (1986) algorithm for the computation of radiated seismic energy, but with the philosophy of a magnitude measurement, i.e., a real-time "quick-and-dirty" single-station estimate ignoring such source details as focal geometry and exact depth.

Specifically, given a seismic record of the vertical ground motion $u(t)$ of a $T$ phase, Okal *et al.* (2003) define

$$TPEF = \rho\alpha \int_W [\dot{u}(t)]^2 \, dt, \tag{5}$$

where $\rho$ and $\alpha$ are the density and $P$-wave velocity of the receiver medium, and $W$ is an appropriate time window containing the $T$ phase. Using Parseval's theorem, *TPEF* can be more readily computed in the Fourier domain as

$$TPEF = \frac{\rho\alpha}{\pi} \int_{\omega_{\min}}^{\omega_{\max}} \omega^2 |U(\omega)|^2 \, d\omega, \tag{6}$$

where the spectral amplitude $U(\omega)$ is the Fourier transform of $u(t)$, and $\omega_{\min}$ and $\omega_{\max}$ are adequate bounds expressing the natural filtering resulting from propagation in the SOFAR channel and seismic recording.

Because of the complexity of the conversion mechanisms near the source and receiver, it is not possible to derive a universal correction and to interpret *TPEF* in terms of the absolute energy radiated by the source into the $T$ phase. Also, such a correction would require a full understanding of the response of the receiving

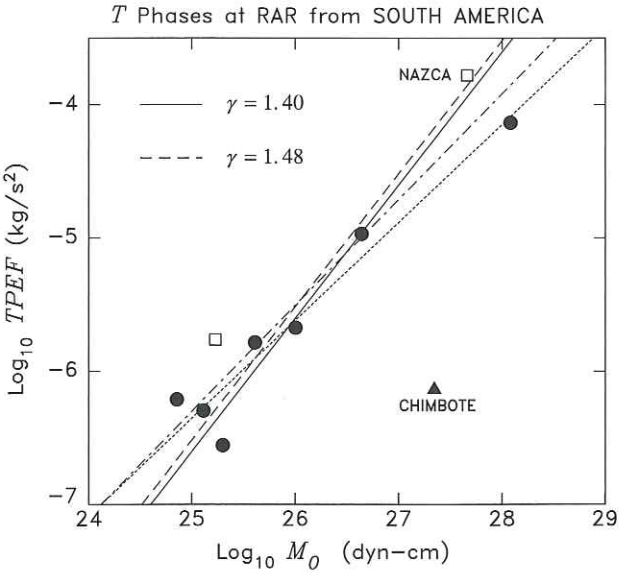


FIG. 16. Correlation between seismic moment $M_0$ and *TPEF*, as recorded at Rarotonga for earthquakes along a 250-km stretch of the coast of Central Chile (solid dots). The dotted line, with a slope of 0.74, is the best linear regression of the dataset of 7 points. The solid line, with a slope constrained to 1, defines the best-fitting value of $\gamma$ (1.40). The two open squares show the large 1996 Nazca event, and one of its strong aftershocks; note that the best regression (dash-dot line, with a slope of 0.79) and the best-fitting $\gamma$ (1.48; long dashes) are essentially unchanged, even though the new events are located in Peru, more than 1000 km away from the original seven. By contrast, the 1996 Chimbote "tsunami earthquake" (triangle) features an extreme deficiency in TPEF of two logarithmic units in $\gamma$, or about six times the scatter in the Chilean data. Adapted (re-labeled) from (Okal *et al.*, 2003).

shore to an acoustic wavetrain, and could therefore depend on such parameters as the back-azimuth of the wavetrain at the station. For this reason, Okal *et al.* (2003) limit the scope of the parameter *TPEF* to the comparison of records obtained at the same station under equivalent receiving conditions, i.e., from similar epicentral areas. In particular, no distance correction is applied in (6).

As in the case of body waves, the quantity *TPEF* would then be expected to scale linearly with seismic moment $M_0$ and thus the parameter $\Gamma = TPEF/M_0$ to remain invariant for sets of comparable seismic sources. (To avoid the use of exceedingly small numbers, we further introduce $\gamma = \log_{10}\Gamma + 30$, where $\Gamma$ is in $\mathrm{cm}^{-2}$.)

This is verified on Fig.16 which examines the relationship between *TPEF* and $M_0$ for ten South American earthquakes recorded at Rarotonga. Note the generally good agreement between the two parameters, suggesting a constant $\gamma$, the only earthquake exhibiting a pronounced deficiency in $\gamma$ (by 1.5 logarithmic units) being the 1996 Chimbote, Peru, "tsunami earthquake". We recall that

Kanamori (1972) defined "tsunami earthquakes" as those events whose tsunamis are much larger than expected from their conventional magnitudes, typical examples being the 1896 Sanriku, 1946 Aleutian, 1975 Kuriles and more recently, 1992 Nicaraguan earthquakes. These have been shown to feature an extremely slow propagation of the rupture along the fault plane, at velocities as low as 1 km/s, itself interpreted as involving rupture in sedimentary wedges (as proposed for Sanriku (Tanioka and Satake, 1996) or Kuriles (Fukao, 1979)), or conversely in a jerky mode along a corrugated fault plane, in the case of a sediment-starved environment such as Nicaragua (Tanioka *et al.*, 1997; Polet and Kanamori, 2000).

The clear violation of source scaling laws by "tsunami earthquakes" is illustrated by their strong $m_b : M_s$ anomalies, recast in more quantitative terms by Newman and Okal (1998) as a deficiency of more than 1 logarithmic unit in the slowness parameter $\Theta = \log_{10}[E^E/M_0]$. Such a source slowness is expected to affect the parameter $\gamma$ as well, and Okal *et al.* (2003) documented that all tsunami earthquakes are strongly deficient generators of $T$ waves, by comparing them with regular events located in the same general area (Fig. 17). The case of the tsunami earthquakes of the 1990s (Nicaragua, 1992; Chimbote, Peru, 1996) for which high-quality digital records are available, is most compelling ($\gamma$ deficient by an average of 1.8 and 1.7 logarithmic units, respectively), but the technique can be extended to analog records in the case of the 1963 Kuriles main aftershock, 1975 Kuriles earthquake and 1982 Tonga event, all of which were described as "tsunami earthquakes" (Fukao, 1979; Talandier and Okal, 1989). Also, Okal *et al.* (2003) and Okal (2004) showed that a faint $T$ wave detected at Hawaii Volcano Observatory in the aftermath of the 1946 Aleutian earthquake arrived too late to be associated with the main shock, and thus confirmed that the latter had not generated a detectable $T$ phase, which further supports its character as an exceptionally slow tsunami earthquake (Kanamori, 1972; López and Okal, 2006).

These results settled a controversy regarding the correlation between $T$-phase excitation and the tsunamigenic character of an earthquake source, which had been longstanding ever since Ewing *et al.* (1950) suggested the use of $T$ phases in tsunami warning, based on the assumption that both kinds of waves would be favored by a very shallow seismic source involving strong coupling with the oceanic column. While their model was disputed by Leet (1951) and Wadati and Inouye (1953), Talandier (1966) and later Walker *et al.* (1992) and Walker and Bernard (1993) have supported the proposed correlation. However, such studies were mostly based on restricted datasets, and predated the large tsunamis of the 1990s, and in particular the "tsunami earthquakes" of 1992 (Nicaragua), 1994 (Java) and 1996 (Chimbote, Peru). As mentioned above, modern developments have rendered Ewing *et al.*'s (1950) model precarious since we now understand that $T$ waves can be generated by the very deepest events (Northrop, 1974; Okal, 2001b), while the generation of far-field tsunami energy is only mildly controlled by source depth for reasonably shallow earthquakes ($h \leqslant 70$ km) (Ward, 1980; Okal, 1988). In addition, Ewing *et al.* (1950) were simply overlooking the extreme

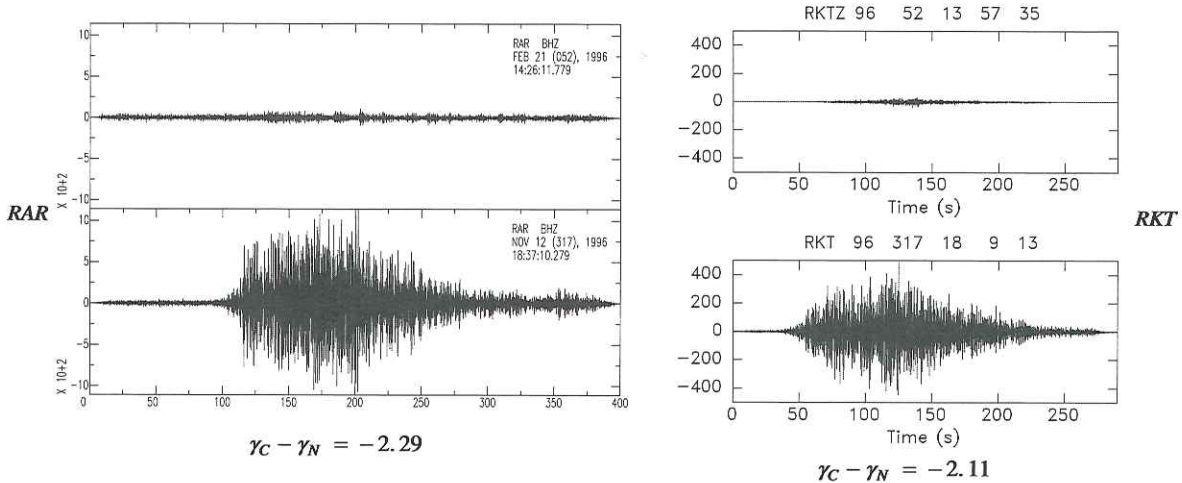


FIG. 17. Comparison of $T$ phases from the Chimbote, Peru "tsunami earthquake" of 21 February 1996 ($M_0 = 2.2 \times 10^{27}$ dyn cm; top frames) and the regular Nazca, Peru event of 12 November 1996 ($M_0 = 4.6 \times 10^{27}$ dyn cm; bottom frames). Vertical scales (in digital units) are arbitrary, but for each station (RAR: Rarotonga, Cook Is.; RPN: Rapa Nui, Easter Is.; RKT: Rikitea, Gambier; PATS: Pohnpei, Caroline Is.), the two $T$ wavetrains are plotted on the same scale. The strong deficiency of the Chimbote $T$ waves is quantified by the difference in the parameters $\gamma$ of the two events at each station. Adapted (re-labeled) from (Okal *et al.*, 2003).

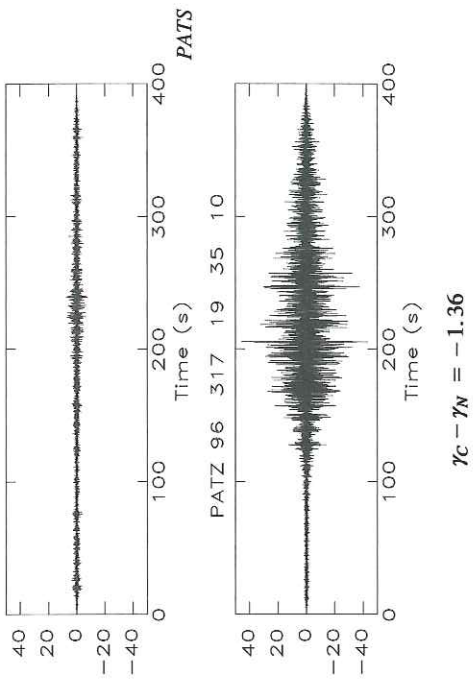


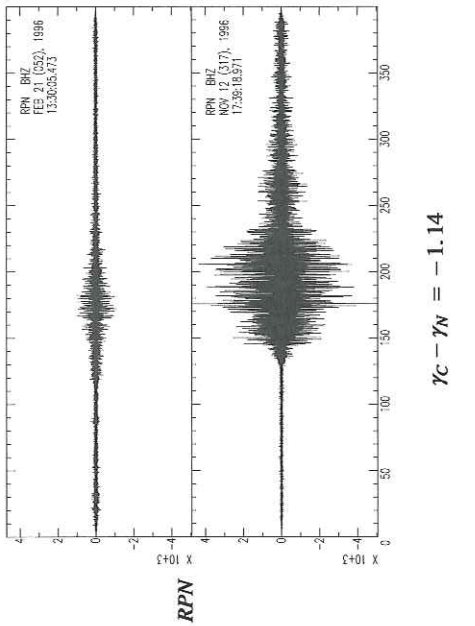


FIG. 17. Continued.

and fundamental difference in the frequencies characteristic of the two types of waves. Indeed, the most efficient tsunami generators, the so-called "tsunami earthquakes", are essentially silent in the acoustic band, just as they often have minimum amplitudes at 1 Hz. As a result, they can remain unfelt by the local residents, who then lack any harbinger of the upcoming disaster, and do not realize the need to urgently evacuate beaches. Such was the tragic case in Nicaragua (1992) where the tsunami killed more than 160 people (Satake *et al.*, 1993), and in Java (1994 and 2006), where the human toll reached 223 and about 700, respectively (Tsuji *et al.*, 1995, Fritz *et al.*, 2007).

The failure of the proposed correlation between the excitation of tsunamis and $T$ waves is further illustrated by the fact that those few earthquakes whose $T$ waves were actually felt at teleseismic distances in the Pacific Basin (the 1958 Fairweather, Alaska, 1977 Tonga, 1994 deep Bolivian and 2003 New Zealand earthquakes; see above) all had at most weak teleseismic tsunamis, while the major catastrophic transpacific tsunamis (1946 Aleutian; 1960 Chile) were not, to our knowledge, accompanied by $T$ waves of sufficient amplitude to be felt in the far field. The 2004 Sumatra $T$ waves were felt in the Maldives, at comparatively short distances.

In conclusion, the concept of the *TPEF* and the associated parameter $\gamma$ can be a powerful tool for the investigation of the dynamic properties of a seismic source. In particular, it proves the deficiency of tsunami earthquakes as $T$-phase generators and establishes firmly this property in the context of seismic source theory, by invoking rupture slowness, itself resulting in a deviation from generally accepted source scaling laws. *TPEF* and hence $\gamma$ involve straightforward, one-station measurements which can be carried out in real time in an observatory environment, and offer immediate insight into the dynamic properties of the source of a distant earthquake.

## The Amplitude-Duration Criterion $D$

In a recent contribution, Talandier and Okal (2001) introduced a source discriminant $D$ comparing the duration and amplitude of teleseismic $T$ wavetrains recorded at island stations. In the context of the monitoring of the CTBT, their motivation was primarily to devise a robust algorithm capable of discriminating between explosive sources in the water column and elastic dislocations in the solid Earth. Specifically, and given the time series $x(t)$ of the ground velocity recorded by a seismic station, they characterize its amplitude through the maximum, $e_{\mathrm{Max}}$, expressed in μm/s, of the envelope $e(t)$ of $x(t)$, after high-pass filtering $x$ above 2 Hz. The duration $\tau_{1/3}$ of the wavetrain is taken as the total time (in s) during which the envelope $e(t)$ maintains a value of at least $\frac{1}{3} e_{\mathrm{Max}}$ (Fig. 18). The discriminant $D$ is then computed as

$$D = \log_{10} e_{\mathrm{Max}} - 4.9 \log_{10} \tau_{1/3} + 4.1. \tag{7}$$

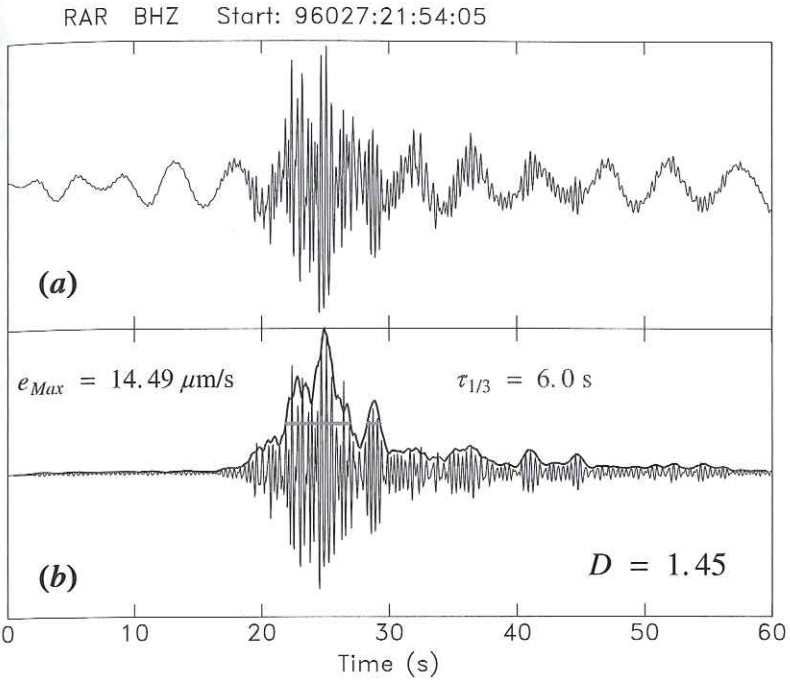


FIG. 18. Computation of the source discriminant $D$ illustrated in the case of the Polynesian nuclear test of 27 January 1996, recorded at Rarotonga. (a): Original broad-band seismogram. (b): Seismogram high-pass filtered at 2 Hz. The thick trace represents the envelope of the record, whose maximum amplitude $e_{\mathrm{Max}}$ is retained. The thick horizontal segments identify those time intervals during which the envelope is sustained at 1/3 of its maximum value (estimated above ambient noise); their total duration is summed to obtain $\tau_{1/3}$. Finally, the discriminant $D$ is computed using (7).

Figure 19 shows that $D$ effectively separates most earthquakes ($D < 0$) from documented explosions ($D > 0$).

In developing this discriminant, Talandier and Okal (2001) were motivated by the failure of several other techniques, applied either in the time or frequency domains, to adequately separate populations of earthquakes and underwater explosions. By comparing an instantaneous measurement (the envelope maximum $e_{\mathrm{Max}}$) and an integrated one (the duration $\tau_{1/3}$), they contrast the high- and low-frequency properties of the source, in a way reminiscent of the time-honored $m_b : M_s$ discriminant used to identify underground explosions based on their classical seismic waves (Marshall and Basham, 1972).

In order to justify the performance of the discriminant $D$, Talandier and Okal (2001) have discussed in very general terms the scaling laws governing the growth with source size of underground dislocations and underwater explosions, and the resulting differences in the power laws controlling the duration and amplitude

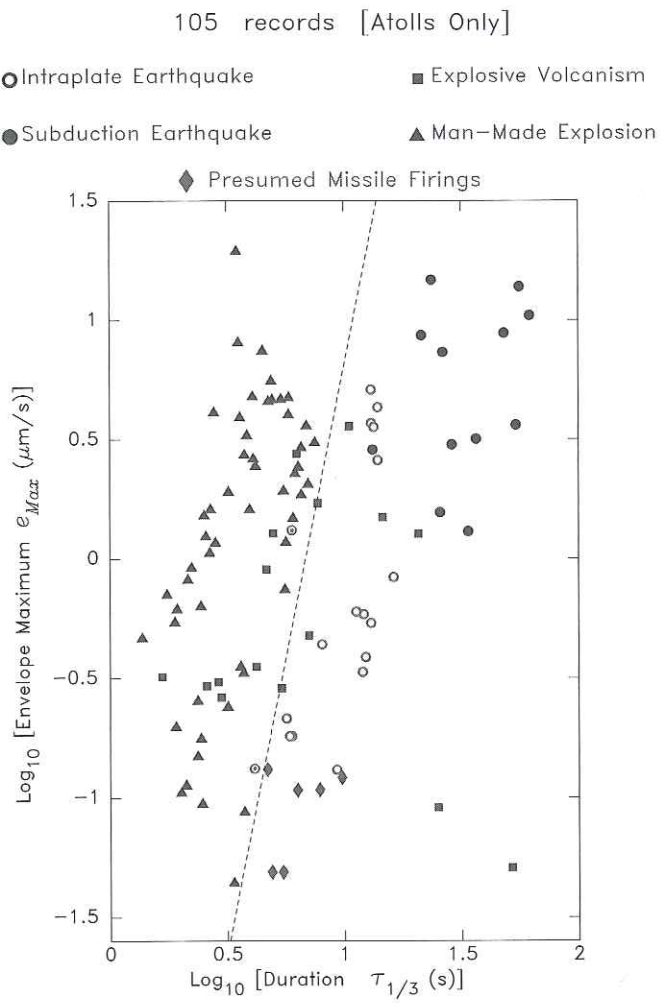


FIG. 19. Performance of the discriminant $D$ (Eq. (7)) for the initial dataset of 105 records at atoll stations studied by Talandier and Okal (2001). The dashed line separates positive and negative values of $D$. Note that all chemical explosions in the oceanic column (triangles) have positive $D$, while most earthquakes (circles) feature negative discriminants. The exceptions (shown as bull's eye symbols) involve two small earthquakes originating in the Hawaiian volcanic structure; see text for details. Adapted (re-labeled) from Talandier and Okal (2001).

of the acoustic wave generated in the SOFAR channel, which indeed lead to a predictable separation of the two populations in the $e_{\mathrm{Max}}$ : $\tau_{1/3}$ plane for large enough sources (magnitude $m_b \geqslant 2$ or yield $Y \geqslant 10$ kg).

We refer to Talandier and Okal (2001) for a full discussion of the operational details of the algorithm, notably regarding the definition of a necessary distance correction, the handling of background noise, the optimization (by trial and error) of the factor 1/3 for the definition of duration, and the preferential use of receiving stations located either on atolls or in the vicinity of a steep, "pali"-like, conversion zone, in order to prevent a long receiver-side upslope conversion from lengthening the wavetrain and diminishing its amplitude.

An important feature of Fig. 19 is the observation that, while documented explosions are well identified by the parameter $D$, the performance of the discriminant is degraded for a small number of earthquakes occurring in the vicinity of intraplate volcanic edifices, such as Hawaii (and Mehetia in the Society Islands), and dubbed "hotspot earthquakes". These events feature an essentially null, or even slightly positive, value of $D$, which Talandier and Okal (2001) explain by noting that, for small earthquakes occurring in the immediate vicinity of the source-side conversion point, the ground motion giving rise to the acoustic wave may belong to the seismological near field, rather than to the far field, and thus violate the scaling laws providing the basis for the discriminant $D$. While this mis-identification of a few intraplate earthquakes may appear as a failure of the proposed discriminant, it actually shows that $D$ is a powerful proxy for the characteristics of $T$-wave sources, and suggests its use to explore systematically the source properties of certain classes of earthquakes.

Note also on Fig. 19 that $D$ fails to identify $T$-phase sources documented as belonging to episodes of underwater volcanic activity. This merely reflects the broad variability of the nature of these sources during the course of a volcanic eruption (e.g., Talandier and Okal, 1987). These may include explosive events, corresponding to the initial unplugging of magmatic conduits, which not surprisingly can share the characteristics of underwater explosions and feature positive values of $D$, as well as slower phenomena occurring later in the sequence and associated with the progression of magma within the conduit and its delivery to the ocean floor; the latter can then feature some of the most negative values of $D$ in Talandier and Okal's (2001) dataset.

Talandier and Okal (2004b) recently complemented their initial study by substantially enlarging their dataset through inclusion of specially targeted families of sources. Among their most significant results, they confirmed the special behavior of many, but not all, "hotspot earthquakes" which show enhanced values of the discriminant $D$ (Fig. 20a). They were able to associate those records featuring positive $D$ with sources in the immediate vicinity of steep conversion zones, which provide an efficient conversion resulting in high amplitudes and short durations.

By contrast, Talandier and Okal (2004b) studied 10 records from true intraplate earthquakes, located in abyssal areas where no significant bathymetry is documented. They all feature negative values of $D$, and are thus unequivocally identified as earthquakes (Fig. 20b). These include some of the most negative $D$

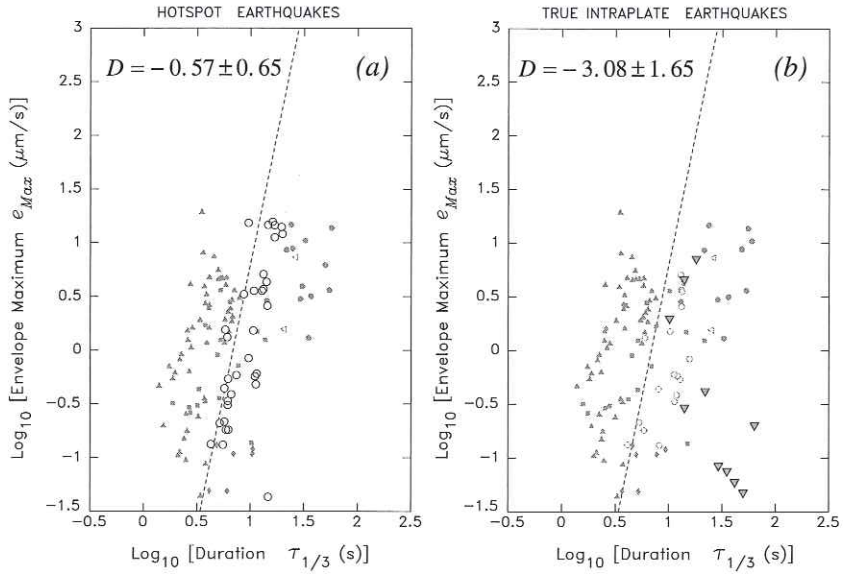


FIG. 20. Discriminant $D$ applied to intraplate earthquakes located inside (or close to) volcanic edifices ("Hotspot earthquakes"; (a): open circles) or in abyssal plains with no known bathymetric features ("True intraplate"; (b): downward-pointing triangles). The background symbols in half-tone are the original dataset from Talandier and Okal (2001). $D = 0$ is shown as the dashed line. Note the occasional positive values of $D$ for hotspot earthquakes, corresponding to sources located close to steep slopes in the volcanic edifice. By contrast, the true intraplate earthquakes all have negative values of $D$, some of them among the lowest measured. After Talandier and Okal (2004b).

values in the authors' catalogue, which expresses the general inefficiency of the scattering mechanisms required for abyssal conversion, especially at the relatively low acoustic frequencies typical of seismic recording. In addition, the delocalization of the scatterers on the ocean floor can contribute to an increase in the duration of the signal, as modeled by deGroot-Hedlin and Orcutt (1999) and Yang and Forsyth (2003). The occasionally larger but still negative values of $D$ shown on Fig. 20b could result from conversions involving an unchartered bathymetric feature.

Figure 21 further compares the properties of $T$ waves generated from earthquakes at the subduction zones of the Pacific "Ring of Fire" and along transform faults of the Pacific Mid-Oceanic Ridge systems. While the average value of $D$ is slightly greater for the latter, there is no clear separation of the two populations. Anomalous events, featuring normal faulting on the Eltanin Transform Faults (Okal and Langenhorst, 2000), are not identifiable within the group. On the other hand, this dataset does support the observation that strike–slip earthquakes (from the Transform Fault dataset) may be nominally more efficient $T$-wave generators than thrust or normal faulting ones, especially at lower magnitudes. Figure 22

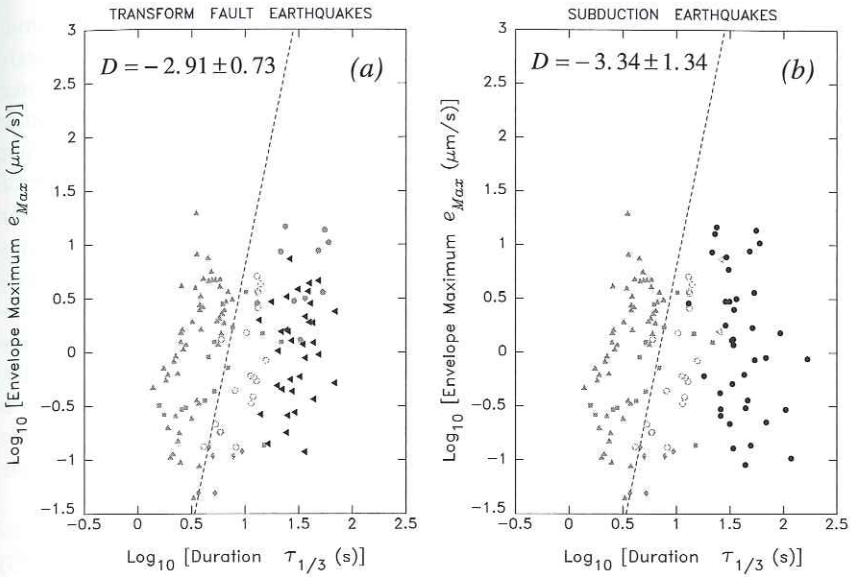


FIG. 21. Comparison of the performance of the discriminant $D$ for 35 records from earthquakes on transform faults ((a): left-pointing triangles) and 53 records of subduction zone events ((b): solid circles). The background symbols in half-tone are the original dataset from Talandier and Okal (2001). $D = 0$ is shown as the dashed line. After Talandier and Okal (2004b).

(Talandier and Okal, 2004b) documents and quantifies this trend on a population of 23 $T$ phases recorded at Rarotonga from the Eltanin and Kurile epicentral areas. These results are generally compatible with those of Dziak (2001), who had first reported this property using hydrophone records of regional events in the area of the Juan de Fuca and Gorda Ridges (Fig. 22a). While the trends of the two datasets are largely similar, the slopes of the best-fitting regressions differ significantly. However, in Talandier and Okal's (2004b) study, the regression slopes had to be computed using body-wave magnitude $m_b$ in the absence of a sufficient number of published moment values, whereas Dziak (2001) used moment magnitudes obtained by inversion of regional waveforms (Nábělek and Xia, 1995). In the relevant range of magnitudes, the slope of $m_b$ vs. $\log_{10} M_0$ is expected to vary between 2/3 ($m_b \leqslant 5$) and 1/3 ($m_b > 5$) (Geller, 1976), and consequently, Talandier and Okal's (2004b) slopes should be adjusted by a factor which could reach 0.5, in order to be compared with those of Dziak (2001). Additional differences between the two studies may reflect the variation in frequency band resulting from the difference in instrumentation.

Park *et al.* (2001) have suggested that the preferential excitation of $T$ waves by strike–slip faults may express the dependence of Rayleigh wave excitation on focal mechanism and depth (e.g., Kanamori and Stewart, 1976). A simple physi-

cal analysis of this conjecture is not forthcoming, as the extremely short seismic wavelengths involved (i.e., the very large equivalent angular orders in the spherical Earth, on the order of $l = 10^4$ to $10^5$ for the modes on Fig. 10) preclude the use of asymptotic expansions valid for shallow sources or in the limit of the seismic near field; note in particular that the scatterers are bound to range several, if not many, wavelengths away from the epicenter. In addition, the apparent decrease of the effect with earthquake size, recognizable in both Dziak's (2001) and Talandier and Okal's (2004b) datasets (Fig. 22), would suggest that source finiteness plays a crucial role; however, its effect on the excitation of seismic surface waves does not lend itself to a simple analysis at very high frequencies, both in the directivity formalism (Ben-Menahem, 1961) or the higher-moment one (Okal, 1982). By contrast, the formalism of Yang and Forsyth (2003) may, at least conceptually, be more directly applicable to further exploring the effect of focal mechanism on the generation of abyssal $T$ waves; at any rate, it is clear that more systematic theoretical investigations will be necessary before the origin of this remarkable observation is fully understood.

Talandier and Okal (2004b) also explored the $T$-wave characteristics of underwater landslides, by considering the case of the Papua New Guinea (PNG) earthquake series of 1998 (Fig. 23). We recall that a major local tsunami, which killed more than 2200 people, was generated following a relatively weak earthquake ($M_0 = 3.7 \times 10^{26}$ dyn cm), which did not feature the slow character of "tsunami earthquakes" (Synolakis *et al.*, 2002). The origin of the tsunami was later attributed to an underwater landslide, triggered 13 minutes after the mainshock and identified from its $T$ wave recorded throughout the Pacific Basin, and in particular on the Wake Island hydrophone (Okal, 2003). The $T$ waveform was exceptionally long, given the small classical magnitude ($m_b = 4.4$) assigned to its source. This can be interpreted as a disparity between amplitude and duration of the source, which we formally examine on Fig. 23, where we plot $D$ values computed from waveforms recorded at the seismic station on Wake Island. In addition to the tsunamigenic slump (with origin time 09:02 GMT on 17 July 1998), the dataset on that figure consists of the 1998 PNG mainshock (08:49), of a number of small aftershocks (09:06, 09:40), and of the mainshock of the 2002 PNG event, which occurred 120 km to the Southeast, was larger than the 1998 earthquake, but generated only a benign tsunami (Borrero *et al.*, 2003). Note that the 09:02 event ($D = -3.55$) effectively features a deficiency in $D$ of more than one logarithmic unit with respect to most of the neighboring events, suggesting a source process of a different physical nature. By contrast, the 1998 and 2002 mainshocks feature comparable values of $D$ ($-1.58$ and $-1.26$ respectively), supporting a commonality of seismic source, which again requires that the catastrophic 1998 tsunami must have been generated by an auxiliary source.

In addition, we point out a small event on 12 December 2002, located 6 km off the southwestern shore of the Island of Hawaii, and featuring $D = -3.18$. While this value is not significantly different from those of truly intraplate earthquakes,

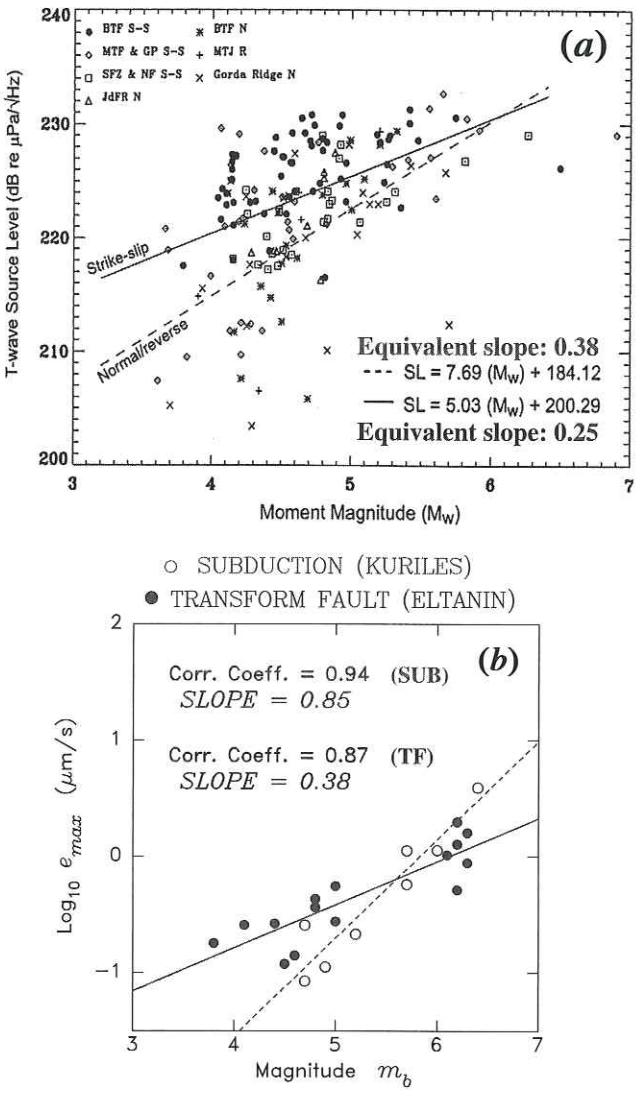


FIG. 22. Preferential excitation of $T$ waves by strike–slip earthquakes. (a): Dziak's (2001) dataset of 179 regional earthquakes recorded on hydrophones in the Northeast Pacific. The regression slopes have been reinterpreted in terms of linear physical units, rather than decibels, as 0.25 (strike–slip) and 0.38 (other), (b): Talandier and Okal's (2004b) dataset of 8 $T$ phases from subduction events in the Kuriles (open symbols; regressed as dashed line), and 15 transform fault earthquakes from the Eltanin Fracture Zone (solid symbols; regressed as solid line), recorded at Rarotonga. Note the generally similar pattern of preferential excitation of $T$ phases by the latter at low magnitudes. See text for discussion. Combination of new material with figure adapted from Dziak (2001).

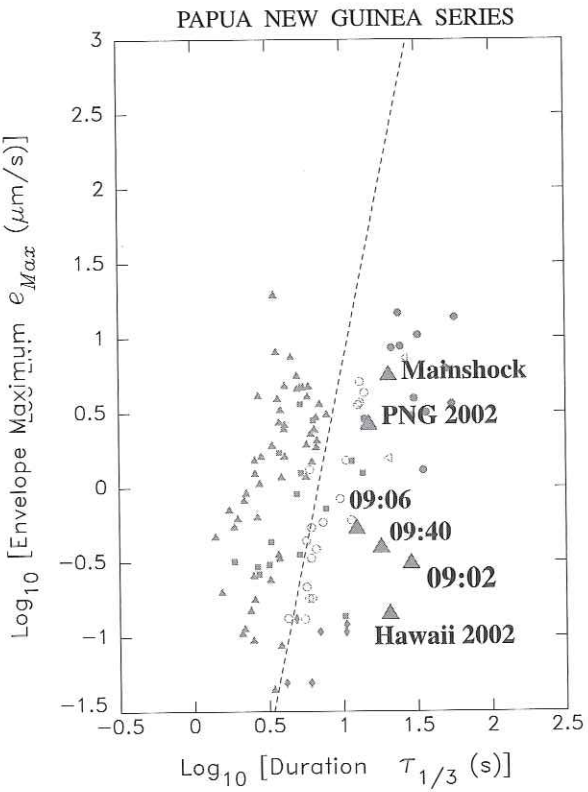


FIG. 23. Discriminant $D$ computed at the Wake Island seismic station for a series of events in Papua New Guinea on 17 July 1998. Note that the 09:02 aftershock, interpreted as a major underwater slump (Synolakis *et al.*, 2002), features a deficit of more than one unit ($D = -3.55$) with respect to neighboring earthquakes. Also shown are the regular event nearby on 08 September 2002, and a small 2002 event near the coast of Hawaii interpreted by Reymond *et al.* (2004) as an underwater landslide. The background symbols in half-tone are the original dataset from Talandier and Okal (2001). $D = 0$ is shown as the dashed line. After Talandier and Okal (2004b).

it is substantially deficient among Hawaiian earthquakes, and reminiscent of that of the 1998 PNG underwater landslide. This observation, and the comparison of the regional seismic waveforms recorded on the island with those of documented subaerial landslides, suggests that the event in question is indeed an underwater landslide, taking place on a steeply sloping section of the island structure identifiable in the local bathymetry (Reymond *et al.*, 2004). This tentative interpretation would support the contention that landslides are probably rather inefficient, if not occasionally silent, sources of hydroacoustic energy, even though their duration may be substantial. Incidentally, such signals differ significantly from those described by Caplan-Auerbach *et al.* (2001) as originating from bench collapses

at the Kilauea eruption ocean entry point and recorded on hydrophones of the autonomous equatorial array (Fox *et al.*, 2001). The latter have much shorter durations, which probably reflects the difference in the nature of the slide (the simple collapse of a cohesive block) and the shorter length of its total underwater path.

Finally, in Fig. 24, we compare on a dataset of eight South American earthquakes the performance of the three parameters $D$, $\gamma$, and $\Theta$, introduced by Talandier and Okal (2001), Okal *et al.* (2003) and Newman and Okal (1998) to detect any possible slowness in the rupture characteristics of seismic sources. The first two are based on the properties of $T$ waves, and the third one on the energy of body waves. The eight events span two logarithmic units of $\Theta$, including both slow earthquakes such as the 1996 Chimbote, Peru "tsunami earthquake", and fast or "snappy" ones such as the Chilean event of 15 October 1997 (Okal and Kirby, 2002). We find remarkable correlations between $\gamma$ and $\Theta$ (86%), and between $D$ and $\gamma$ (84%), and a spectacular one (98%) between $D$ and $\Theta$. In particular, the 1996 Chimbote, Peru earthquake features the lowest value of $D$ ($-7.03$) measured by Talandier and Okal (2004b). The 2001 Peruvian mainshock, identified as trending toward slowness (Okal *et al.*, 2002) also features a low value of $D$, and to a lesser extent, of $\gamma$. By contrast, all three "snappy" earthquakes with large values of $\Theta$ also have high parameters $\gamma$ and $D$. These include the two deeper than normal intraplate events in Chile and the normal faulting Peruvian shock triggered on 05 July 2001 by stress transfer from the Peruvian mainshock.

These observations serve to confirm, if need be, that $D$ can be a reliable descriptor of the source properties of an earthquake, and more generally that the $T$-phase waveform carries valuable information on the source properties of earthquakes, which can be extracted through the use of analytical algorithms paralleling the methodologies traditionally utilized on conventional seismic waves.

## The Case of the 2004 Sumatra Earthquake

With a seismic moment of at least $10^{30}$ dyn cm (Stein and Okal, 2005; Tsai *et al.*, 2005), the disastrous Sumatra–Andaman earthquake of 26 December 2004 was the largest one in 40, and perhaps 44, years. A fascinating aspect of this event is that its recordings transcended the conventional boundaries of instrumentation. For example, its tsunami was recorded by technologies as diverse as satellite altimetry (Scharroo *et al.*, 2005), infrasound (Le Pichon *et al.*, 2005), hydrophones of the International Monitoring System (IMS) of the CTBT Organization (Hanson and Bowman, 2005), detection of ionospheric perturbation using arrays of GPS recorders (Occhipinti *et al.*, 2005), and even on the horizontal components of near-shore broadband seismometers at teleseismic distances (Yuan *et al.*, 2005; Okal, 2007). In this context, and given the unique character of the earthquake, a description of its $T$ waves is in order.

The source characteristics of the Sumatra earthquake were investigated in the framework of the parameters $\gamma$ and $D$ introduced above. In this respect, we recall

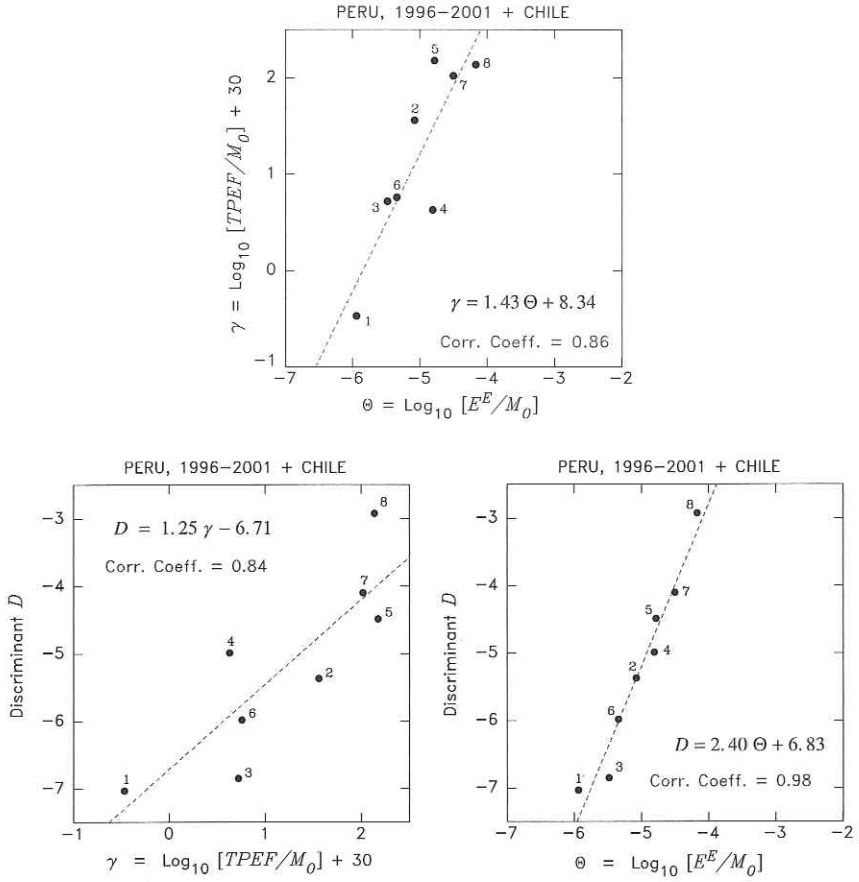


| Number | Date | Event | Remarks |
|---|---|---|---|
| 1 | 1966:052 | Chimbote, Peru | Tsunami Earthquake |
| 2 | 1996:317 | Nazca, Peru | |
| 3 | 2001:174 | Peru, Main shock | |
| 4 | 2001:177 | Peru, First Large Aftershock | |
| 5 | 2001:186 | Peru, Triggered Normal Faulting | Snappy |
| 6 | 2001:188 | Peru, Largest Aftershock | |
| 7 | 1997:288 | Ovalle, Chile | Snappy (Okal and Kirby, 2002) |
| 8 | 1998:210 | Chile (Outboard, Intraplate) | Snappy |

FIG. 24. Correlation between various scale-invariant measures of the slowness of an earthquake source, investigated on $T$ wave records at Rarotonga of eight South American earthquakes, listed in the box. *Top*: Parameter $\gamma$ *vs.* slowness parameter $\Theta$ introduced by Newman and Okal (1998). *Center left*: Discriminant $D$ vs parameter $\gamma$. *Center right*: Discriminant $D$ *vs.* $\Theta$. Note the excellent correlations, especially in the latter case. See text for detailed interpretation.

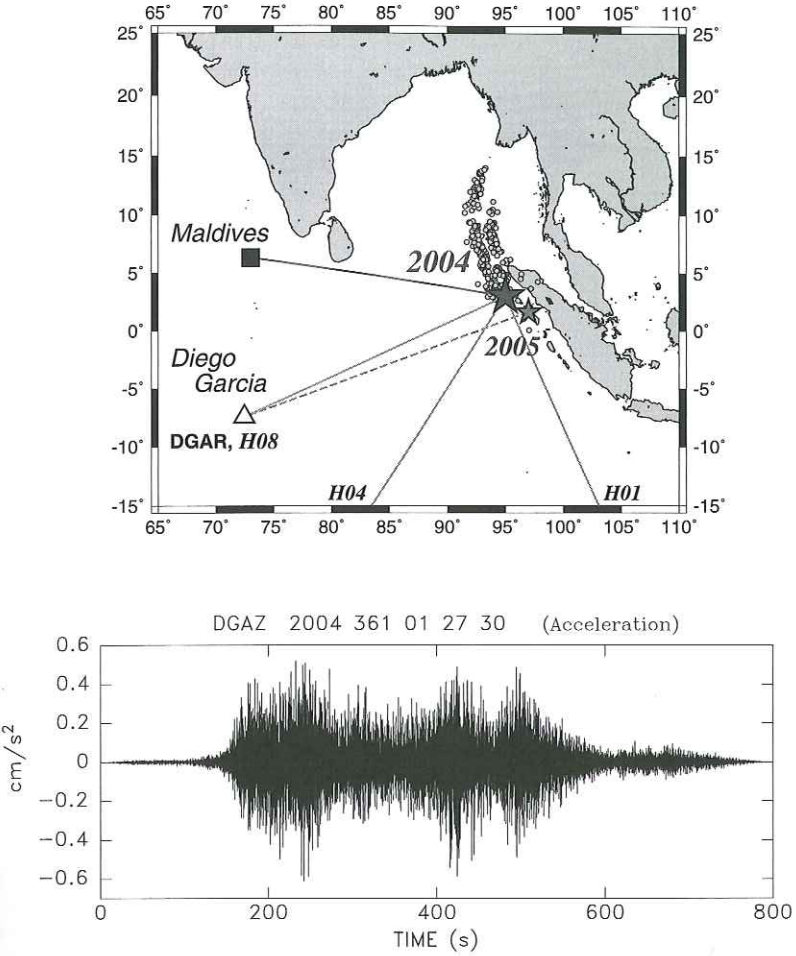


FIG. 25. *Top*: Map of the Northeastern Indian Ocean Basin showing the 2004 and 2005 Sumatra events (stars) and paths of $T$ phases to the Maldives and Diego Garcia, with partial rays to Crozet (H04) and Cape Leeuwin (H01). The small symbols represent the same-day aftershocks of the 2004 Sumatra earthquake, and illustrate the extent of the fault rupture. *Bottom*: Accelerogram of the $T$ phase deconvolved from the broadband seismometer record at the seismic station DGAR on Diego Garcia. Note that the duration of the record does not extend beyond 450 seconds.

that only relative evaluations at the same receiver are legitimate, and proceed to compare the $T$ wavetrains recorded at the seismic station DGAR on Diego Garcia atoll from the 2004 Sumatra–Andaman earthquake and the Simeulue–Nias event of 28 March 2005 to the Southeast (Fig. 25). At $M_0 = 1.1 \times 10^{29}$ dyn cm, the latter, apparently triggered by Coulomb stress transfer from the 2004 event

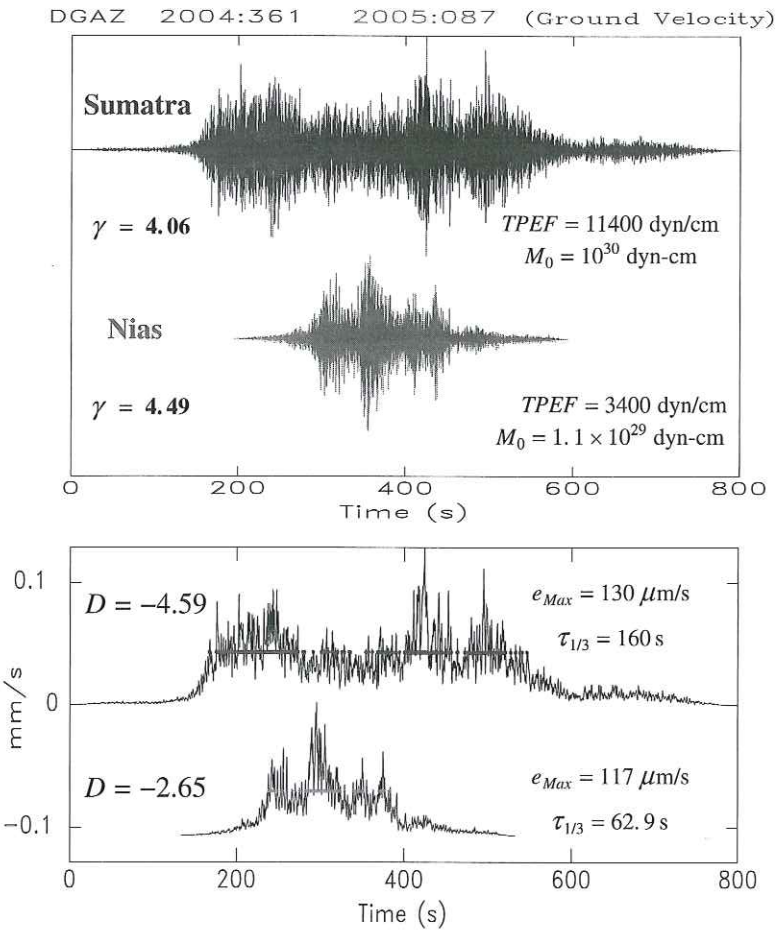


FIG. 26. Analysis of $T$ phases recorded at the seismic station DGAR (Diego Garcia) from the two large 2004 and 2005 Sumatra earthquakes. *Top*: Broadband seismograms high-pass filtered at 2 Hz (yielding essentially ground velocity) plotted on common time and amplitude scales, with parameters relevant to the calculation of *TPEF* and $\gamma$. *Bottom*: Calculation of the discriminant $D$. Note the relatively comparable values of $e_{\mathrm{Max}}$, but the very much longer $\tau_{1/3}$ in the case of the 2004 event, resulting in a much lower value of $D$.

(McCloskey *et al.*, 2005) is itself truly gigantic, and would have been the largest recorded event since 1965, if not for the 2004 Sumatra earthquake. Figure 26 compares the relevant waveforms and demonstrates a significant difference (of more than two units) in the discriminants $D$. Note that the Northern extremity of the 2004 rupture is generally masked in the direction of Diego Garcia, resulting in a somewhat shortened $T$ wave, not exceeding 450 s in duration (Fig. 25),

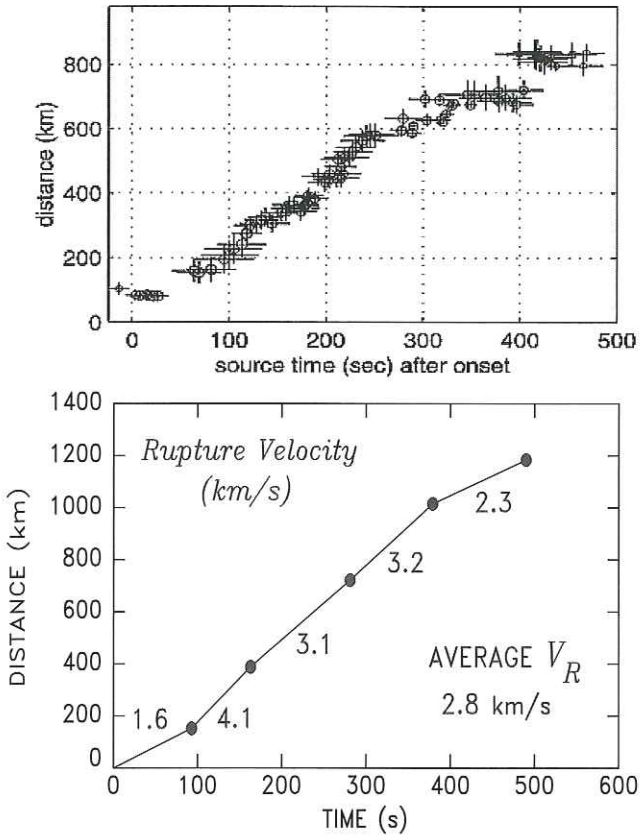


FIG. 27. Source tomography of the 2004 Sumatra earthquake. *Top*: Time history of the progression of the rupture along the fault line as mapped by backtracking beamed signals from Indian Ocean hydrophone arrays (deGroot-Hedlin, 2005). *Bottom*: Spaciotemporal evolution of the components of the multi-source CMT inversion of mantle waves by Tsai *et al.* (2005). The two diagrams use the exact same scales, allowing direct comparison. Note the remarkable agreement, especially regarding the slowing down of the rupture to the North, and also the tentatively slow initiation of the rupture in the South. Adapted (combined; re-scaled; re-labeled) from deGroot-Hedlin (2005) and Tsai *et al.* (2005).

rather than the generally accepted value of at least 500 s obtained from seismic source tomography (Ishii *et al.*, 2005). This also results in an underestimation of $\tau_{1/3}$, which would suggest an even more deficient value of $D$. By contrast, the Simeulue–Nias 2005 earthquake featured bilateral rupture (Walker *et al.*, 2005), resulting in an increased value of $D$. As for the parameters $\gamma$ of the two events, they are found largely comparable.

$T$ waves from the 2004 Sumatra earthquake were also recorded by hydrophones of the IMS; by a stroke of luck, the deployment of the hydrophone part of the sys-

tem started with the Indian Ocean sites, with stations operational in 2004 at Diego Garcia (H08), Crozet (H04) and Cape Leeuwin (H01). The availability of triads of hydrophones then allowed directional beaming of the signals using sophisticated techniques, like the PMCC method (Cansi, 1995), which tracks parameters such as incident azimuth, frequency, signal strength and coherence among array sites, as a function of time in the wave packet. By back-tracking this information to the source, $T$ waves were successfully used in a series of studies (deGroot-Hedlin, 2005; Guilbert *et al.*, 2005; Tolstoy and Bohnenstiehl, 2005) to map the progression of the acoustic source, and hence of the earthquake rupture along the fault plane, in what amounted to the first applications of $T$ phases to detailed earthquake source tomography. These studies confirmed the large spatial extent and long duration of the source, and documented a generally slow, but subtly variable, rupture velocity (Fig. 27). Note that because of the slower propagation velocity of $T$ waves in the ocean, hydroacoustic signals offer in this respect a better resolution than comparable algorithms based on conventional body waves, such as used by Ishii *et al.* (2005) and Ohrnberger and Krüger (2005). The rupture velocity (on the average 2.7 km/s) was found to be significantly deficient with respect to that predicted by scaling laws (typically 3.5 km/s), but without reaching the very slow velocities, generally less than 2 km/s, typical of "tsunami earthquakes" (Polet and Kanamori, 2000; López and Okal, 2006). The emerging picture for the 2004 Sumatra event is that of a definitive trend towards slowness, but falling short of the truly anomalous behavior of the classic tsunami earthquakes, a property also confirmed by Weinstein and Okal's (2005) analysis of the parameter $\Theta$ of the 2004 earthquake.

In this context, it is interesting to note that tremors were reported widely felt in the Maldives around 06:30 local time (GMT + 5), which coincides with the predicted arrival time of $T$ waves. There was no seismic station operational on the Maldives, but the $T$ phases recorded at DGAR on Diego Garcia, 1530 km to the South (Fig. 25), correspond to a maximum ground acceleration of 0.5 cm/s$^2$. This is slightly below the generally accepted threshold for feeling by humans (1 cm/s$^2$), but we note the unfavorable recording conditions at DGAR, where the seismic station faces the Southeastern shore, thus requiring a significant land path for the converted seismic wave. It is thus almost certain that the Sumatra $T$ waves were felt in the Maldives, four hours before the arrival of the tsunami, and in hindsight that their correct interpretation could have led to a warning of the population of this atoll nation, which suffered about 100 casualties. In this respect, the 2004 Sumatra earthquake may be the only reported case of an earthquake having generated a catastrophic oceanwide tsunami, and which had been felt in the far field through its $T$ waves. The fact that the $T$ waves were of high enough amplitude to be felt is also consistent with the relatively high value of $\gamma$, relative to the 2005 event: the 2004 earthquake did release significant amounts of high-frequency energy which found its way into $T$ waves, and it was anomalous only in that its source lasted longer than expected, even for an event of its size. These remarks

further illustrate the different source characteristics controlling the parameters $D$ and $\gamma$.

## 6. Conclusion

In conclusion of this review, it is interesting to reflect on the role of earthquake-generated $T$ phases in the development of hydroacoustics. Underwater explosions obviously constitute simpler sources of acoustic energy in the ocean, and indeed have been used in a broad range of calibration experiments, including Worzel and Ewing's (1948), Weigel's (1990), and more recently Blackman *et al.*'s (2003).

However, the ubiquitous character of earthquake sources, both in space and time, has made them the primary tool of the steady progress of our command of hydroacoustics in the past 70 years. In this respect, and from the strict standpoint of unclassified geophysical research, several eras emerge as milestones, which can be conveniently identified by the individual laboratories where the crucial developments took place.

- The Lamont years (1950s), under the leadership of W. Maurice Ewing, saw the emergence of the fundamental picture, establishing firmly the nature of the $T$ wave and the relevant interactions between seismic and acoustic waves at source and receiver slopes. The resulting model would pave the way for a decade of glorified applications of standard geometrical optics.
- The Hawaii years (1960s) involved the operation of a Pacific-wide array of hydrophones by the Hawaii Institute of Geophysics. Some of the most far-reaching results obtained by R.H. Johnson included the discovery of Macdonald Seamount, and the identification of the limits of validity of strict geometrical optics. The dataset collected was truly massive by those days' standards, and would fuel many years of seminal studies, notably by D.A. Walker, on various topical subjects. However, the 1970s and 1980s did not see major developments in instrumentation.
- The PMEL years (1990s) resulted from partial declassification of SOSUS, which allowed C.G. Fox to detect and monitor in real time an episode of volcanic eruption on a segment of the Mid-Oceanic Ridge system. In turn, this led to the development and deployment of the autonomous arrays in the vicinity of the East Pacific in Mid-Atlantic Ridges.
- The 2000s should become the years of the International Monitoring System (IMS), as hydroacoustics were defined in 1996 as one of four technologies to be used in the monitoring of the CTBT, which mandated the deployment of six hydrophones and five land-based seismic T-phase stations. While hydroacoustic monitoring is clearly aimed at the detection of man-made events in the water column, the growing database flowing from the IMS stations

(and from other networks such as the autonomous arrays and the RSP) emanates primarily from natural sources, some of which would not have been envisioned a decade ago, e.g., cryosignals generated by calving or drifting icebergs (Talandier *et al.*, 2002, 2006). However, earthquakes remain a premium source of hydroacoustic energy, and the new detection capabilities provided by the implementation of the IMS will allow the furtherance of our understanding of earthquake sources in the oceanic environment, notably through the use of the analytical methods being developed to interpret the hydroacoustic spectrum in terms of source properties.

In this context, $T$ waves are truly coming of age as an equal partner to conventional seismic waves.

## ACKNOWLEDGEMENTS

I am grateful to Ralph Stephen and Robert Odom, conveners of the workshop on "Seismo-acoustic applications in Marine Geology and Geophysics", held at Woods Hole in March 2004, for inviting me to present a keynote lecture, and encouraging me to write up a review paper on its topic. My work on $T$ phases has benefited from many years of regular cooperation with the Commissariat à l'Energie Atomique (France), and particularly from joint research with Jacques Talandier, Dominique Reymond and Olivier Hyvernaud. Several aspects of $T$-phase quantification were supported by the Department of Defense, most recently under Contract DTRA01-00-C-0065, and regarding tsunami hazard by the National Science Foundation, under Grant CMS-03-01054. I thank Library Staff at Northwestern University, the University of Chicago and Harvard University for help with the retrieval of historical references. Most maps were drafted using the GMT software (Wessel and Smith, 1991).

## REFERENCES

Adams, R.D. (1979). $T$-phase recordings at Rarotonga from underground nuclear explosions. *Geophys. J. Roy. Astr. Soc.* **58**, 361–369.

Bard, P.-Y., Campillo, M., Chavez-García, F.J., Sanchez-Sesma, F. (1988). The Mexico earthquake of September 19, 1985; A theoretical investigation of large- and small-scale amplification effects in the Mexico City valley. *Earthq. Spectra* **4**, 609–633.

Båth, M., Shahidi, M. (1971). $T$ phases from Atlantic earthquakes. *Pure Appl. Geophys.* **92**, 74–114.

Ben-Menahem, A. (1961). Radiation of seismic surface waves from finite moving sources. *Bull. Seismol. Soc. Amer.* **51**, 401–435.

Ben-Menahem, A., Toksöz, M.N. (1963). Source mechanism from spectra of long-period seismic surface waves. 3. The Alaska earthquake of July 10, 1958. *Bull. Seismol. Soc. Amer.* **53**, 905–919.

Biot, M.A. (1952). The interaction of Rayleigh and Stoneley waves in the ocean bottom. *Bull. Seismol. Soc. Amer.* **42**, 81–93.

Blackman, D.K., Mercer, J.A., Andrew, R., deGroot-Hedlin, C.D., Harben, P.E. (2003). Indian Ocean Calibration tests: Cape Town–Cocos Keeling, 2003. In: Proc. 25th Seismic Res. Review – Nuclear Monitoring: Building the Knowledge Base, Tucson, AZ, September 23–25, 2003, pp. 517–523. Nat. Nuclear Security Admin. (abstract).

Boatwright, J., Choy, G.L. (1986). Teleseismic estimates of the energy radiated by shallow earthquakes. *J. Geophys. Res.* **91**, 2095–2112.

Bohnenstiehl, D.R., Tolstoy, M., Dziak, R.P., Fox, C.G., Smith, D.K. (2002). Aftershock sequences in the mid-ocean ridge environment: an analysis using hydroacoustic data. *Tectonophysics* **354**, 49–70.

Bohnenstiehl, D.R., Tolstoy, M., Smith, D.K., Fox, C.G., Dziak, R.P. (2003). Time-clustering behavior of spreading-center seismicity between 15 and 35° N on the Mid-Atlantic Ridge: observations from hydroacoustic monitoring. *Phys. Earth Planet. Inter.* **138**, 147–161.

Borrero, J.C., Bu, J., Saiang, C., Uslu, B., Freckman, J., Gomer, B., Okal, E.A., Synolakis, C.E. (2003). Field survey and preliminary modeling of the Wewak, Papua New Guinea earthquake and tsunami of September 9, 2002. *Seismol. Res. Lett.* **74**, 393–405.

Brekhovskikh, L.M. (1949). O rasprostranenii zvuka v podvodnom zvukovom kanale. *Dokl. Akad. Nauk SSSR* **69**, 157–160 (in Russian).

Brekhovskikh, L.M., Lysanov, Yu. (1982). Fundamentals of Ocean Acoustics. Springer-Verlag, Berlin, 250 pp.

Brune, J.N. (1964). Travel times, body waves, and normal modes of the Earth. *Bull. Seismol. Soc. Amer.* **54**, 2099–2128.

Butler, R., Lomnitz, C. (2002). Coupled seismoacoustic modes on the seafloor. *Geophys. Res. Lett.* **29** (10), 571–574.

Cansi, Y. (1995). An automatic seismic event processing for detection and location: The P.M.C.C. method. *Geophys. Res. Lett.* **22**, 1021–1024.

Cansi, Y., Béthoux, N. (1985). $T$ waves with long inland paths: Synthetic seismograms. *J. Geophys. Res.* **90**, 5459–5465.

Caplan-Auerbach, J., Fox, C.G., Duennebier, F.K. (2001). Hydroacoustic detection of submarine landslides on Kilauea Volcano. *Geophys. Res. Lett.* **28**, 1811–1813.

Colladon, J.D., Sturm, J.K.F. (1827). La vitesse du son dans les liquides. *Annales de Chimie et de Physique, Série 2* **36**, 236–257.

Collins, M.P. (1936). Bulletin Number 5, Harvard University Seismograph Station, 5, 23 pp.

Coulomb, J., Molard, P. (1949). Ondes séismiques au fond de la mer des Antilles. *Ann. Geophys.* **5**, 212–214.

Coulomb, J., Molard, P. (1952). Propagation des ondes séismiques $T$ dans la mer des Antilles. *Ann. Géophys.* **8**, 264–266.

deGroot-Hedlin, C.D. (2005). Estimation of the rupture length and velocity of the great Sumatra earthquake of Dec 26, 2004 using hydroacoustic signals. *Geophys. Res. Lett.* **32** (11), L11303, 4 pp.

deGroot-Hedlin, C.D., Orcutt, J.A. (1999). Synthesis of earthquake-generated $T$ waves. *Geophys. Res. Lett.* **26**, 1227–1230.

Dietz, R.S., Sheehy, M.J. (1954). Transpacific detection of Myojin Volcanic eruptions by underwater sound. *Geol. Soc. Amer. Bull.* **65**, 942–956.

Duennebier, F.K., Johnson, R.H. (1967). $T$-phase sources and earthquake epicenters in the Pacific Basin, *Hawaii Inst. Geophys. Rept.* 67–24, Univ. Hawaii, Honolulu, 104 pp.

Dziak, R.P. (2001). Empirical relationship of $T$-wave energy and fault parameters of Northeast Pacific ocean earthquakes. *Geophys. Res. Lett.* **28**, 2537–2540.

Dziak, R.P., Fox, C.G., Schreiner, A.E. (1995). The June–July 1993 seismo-acoustic event at CoAxial segment, Juan de Fuca Ridge: Evidence for a lateral dike injection. *Geophys. Res. Lett.* **22**, 135–138.

Eaton, J.P., Richter, D.H., Ault, W.U. (1961). The tsunami of May 23, 1960 on the island of Hawaii. *Bull. Seismol. Soc. Amer.* **51**, 135–157.

Embley, R.W., Chadwick Jr., W.W., Jonasson, I.R., Butterfield, D.A., Baker, E.T. (1995). Initial results of the rapid response to the 1993 CoAxial event: Relationships between hydrothermal and volcanic processes. *Geophys. Res. Lett.* **22**, 143–146.

Ewing, W.M., Worzel, J.L. (1948). Long-range sound transmission. *Geol. Soc. Amer. Mem.* **27**. Part 3, 39 pp.

Ewing, W.M., Woollard, G.P., Vine, A.C., Worzel, J.L. (1946). Recent results in submarine geophysics. *Geol. Soc. Amer. Bull.* **57**, 909–934.

Ewing, W.M., Tolstoy, I., Press, F. (1950). Proposed use of the $T$ phase in tsunami warning systems. *Bull. Seismol. Soc. Amer.* **40**, 53–58.

Ewing, W.M., Press, F., Worzel, J.L. (1952). Further study of the $T$ phase. *Bull. Seismol. Soc. Amer.* **42**, 37–51.

Ewing, W.M., Jardetzky, W.S., Press, F. (1957). Elastic Waves in Layered Media. McGraw-Hill, New York, 380 pp.

Fischer, K.M., McCann, W.R. (1984). Velocity modeling and earthquake relocation in the Northeast Caribbean. *Bull. Seismol. Soc. Amer.* **74**, 1249–1262.

Forsyth, D.W., Yang, Y., Mangriotis, M.-D., Shen, Y. (2003). Coupled seismic slip on adjacent oceanic transform faults. *Geophys. Res. Lett.* **30** (12), 201–204.

Fox, C.G., Dziak, R.P., Matsumoto, H., Schreiner, A.E. (1994). Potential for monitoring low-level seismicity on the Juan de Fuca Ridge using military hydrophone arrays. *Mar. Tech. Soc. J.* **27** (4), 22–30.

Fox, C.G., Radford, W.E., Dziak, R.P., Lau, T.-K., Matsumoto, H., Schreiner, A.E. (1995). Acoustic detection of a seafloor spreading episode on the Juan de Fuca Ridge using military hydrophone arrays. *Geophys. Res. Lett.* **22**, 131–134.

Fox, C.G., Matsumoto, H., Lau, T.-K.A. (2001). Monitoring Pacific Ocean seismicity from an autonomous hydrophone array. *J. Geophys. Res.* **106**, 4183–4206.

Fritz, H.M. and 17 co-authors (2007). Extreme runup from the 17 July 2006 Java tsunami. *Geophys. Res. Lett.* **34** (2), L12602, 5 p.

Fukao, Y. (1979). Tsunami earthquake and subduction processes near deep sea trenches. *J. Geophys. Res.* **84**, 2303–2314.

Geller, R.J. (1976). Scaling relations for earthquake source parameters and magnitudes. *Bull. Seismol. Soc. Amer.* **66**, 1501–1523.

Gilbert, F. (1970). Excitation of the normal modes of the Earth by earthquake sources. *Geophys. J. Roy. Astr. Soc.* **22**, 223–226.

Guilbert, J., Vergoz, J., Schisselé, E., Roueff, A., Cansi, Y. (2005). Use of hydroacoustic and seismic arrays to observe rupture propagation and source extent of the $M_w = 9.0$ Sumatra earthquake. *Geophys. Res. Lett.* **32** (15), L15310, 5 pp.

Gutenberg, B. (1957). Effects of ground on earthquake motion. *Bull. Seismol. Soc. Amer.* **47**, 221–250.

Hammond, S.R., Walker, D.A. (1991). Ridge event detection: $T$-phase signals from the Juan de Fuca spreading center. *Mar. Geophys. Res.* **13**, 331–348.

Hanson, J.A., Bowman, J.R. (2005). Dispersive and reflected tsunami signals from the 2004 Indian Ocean tsunami observed on hydrophones and seismic stations. *Geophys. Res. Lett.* **32** (17), L17608, 5 pp.

Harkrider, D.G. (1964). Surface waves in multilayered elastic media. Part I: Rayleigh and Love waves from buried sources in a multilayered elastic half-space. *Bull. Seismol. Soc. Amer.* **54**, 627–679.

Haskell, N.A. (1953). The dispersion of surface waves in multilayered media. *Bull. Seismol. Soc. Amer.* **43**, 17–34.

Hiyoshi, Y., Walker, D.A., McCreery, C.S. (1992). $T$-phase data and regional tsunamigenesis in Japan. *Bull. Seismol. Soc. Amer.* **82**, 2213–2223.

Isacks, B.L., Molnar, P. (1971). Distribution of stresses in the descending lithosphere from a global survey of focal-mechanism solutions of mantle earthquakes. *Rev. Geophys. Space Phys.* **9**, 103–174.

Ishii, M., Shearer, P., Houston, H., Vidale, J. (2005). Rupture extent, duration and speed of the 2004 Sumatra–Andaman earthquake imaged by the Hi-Net array. *Nature* **435**, 933–936.

Jaggar, T.A. (1930). How the seismograph works. *The Volcano Letter* **268**, 1–4.

Jensen, F.B., Kuperman, W.A., Porter, M.B., Schmidt, H. (1994). Computational Ocean Acoustics. AIP Press, Woodbury, NY, 612 pp.

Johnson, R.H. (1970). Estimating earthquake rupture length from $T$ waves. In: Adams, W.A. (Ed.), *Tsunamis in the Pacific Ocean*. Univ. Hawaii, Honolulu, pp. 253–259.

Johnson, R.H., Norris, R.A. (1968). $T$-phase radiators in the Western Aleutians. *Bull. Seismol. Soc. Amer.* **58**, 1–10.

Johnson, R.H., Northrop, J. (1966). A comparison of earthquake magnitude with T-phase strength. *Bull. Seismol. Soc. Amer.* **56**, 119–124.

Johnson, R.H., Northrop, J., Eppley, R. (1963). Sources of Pacific $T$ phases. *J. Geophys. Res.* **68**, 4251–4260.

Johnson, R.H., Norris, R.A., Duennebier, F.K. (1968). Abyssally generated $T$ phases. *Amer. Geophys. Un. Geophys. Monog.* **12**, 70–78.

Kanamori, H. (1972). Mechanisms of tsunami earthquakes. *Phys. Earth Planet. Inter.* **6**, 346–359.

Kanamori, H., Stewart, G.S. (1976). Mode of the strain release along the Gibbs fracture zone, Mid-Atlantic Ridge. *Phys. Earth Planet. Inter.* **11**, 312–332.

Keenan, R.E., Merriam, L.R.L. (1991). Artic abyssal $T$ phases: Coupling seismic energy to the ocean sound channel via under-ice scattering. *J. Acoust. Soc. Amer.* **89**, 1128–1133.

Kennett, B.L.N. (1983). Seismic Wave Propagation in Stratified Media. Cambridge Univ. Press, 342 pp.

Kirby, S.H., Okal, E.A., Engdahl, E.R. (1995). The 09 June 1994 great Bolivian deep earthquake: An exceptional deep earthquake in an extraordinary subduction zone. *Geophys. Res. Lett.* **22**, 2233–2236.

Kuwahara, S. (1939). Velocity of sound in sea water and calculation of the velocity for use in sonic sounding. *Hydrog. Rev.* **16**, 123–140.

Lamb, H. (1904). On the propagation of tremors over the surface of an elastic solid. *Phil. Trans. Roy. Soc. London, Ser. A* **203**, 1–42.

Langevin, P. (1924). The employment of ultra-sonic waves for echo sounding. *Hydrog. Rev.* **2**, 57–91.

Lee, W.H.K., Bennett, R.E., Meagher, K.L. (1972). A method of estimating magnitude of local earthquakes from signal duration, U.S. Geol. Surv. Open File Rept., 28 pp.

Leet, L.D. (1951). Discussion of 'Proposed use of the $T$ phase in tsunami warning systems'. *Bull. Seismol. Soc. Amer.* **41**, 165–167.

Leet, L.D., Linehan, S.J., Berger, P.R. (1951). Investigations of the $T$ phase. *Bull. Seismol. Soc. Amer.* **41**, 123–141.

Leonard, M. (2004). $T$-phase perception: The August 2003, $M_w = 7.1$ New Zealand earthquake felt in Sydney, 1800 km away. *Seismol. Res. Lett.* **75**, 475–480.

Le Pichon, A., Kerry, P., Mialle, P., Vergoz, J., Brachet, N., Garcés, M., Drob, D., Ceranna, L. (2005). Infrasound associated with 2004–2005 large Sumatra earthquakes and tsunami. *Geophys. Res. Lett.* **32** (19), L19802. 5 pp.

Levitus, S., Boyer, T.P., Antonov, J., Burgett, R., Conkright, M.E. (1994). World Ocean Atlas 1994, NOAA/NESDIS, Silver Springs, MA.

Linde, A.T., Gladwin, M.T., Johnston, M.S., Gwyther, R.L., Bilham, R.G. (1996). A slow earthquake sequence on the San Andreas Fault. *Nature* **383**, 65–68.

Linehan, D.S.J. (1940). Earthquakes in the West Indian region. *Trans. Amer. Geophys. Un.* **21**, 229–232.

López, A.M., Okal, E.A. (2006). A seismological reassessment of the source of the 1946 Aleutian "tsunami" earthquake. *Geophys. J. Int.* **165**, 835–849.

Love, A.E.H. (1911). Some Problems of Geodynamics. Cambridge Univ. Press, 180 pp.

Marshall, P.D., Basham, P.W. (1972). Discrimination between earthquakes and underground explosions using an improved $M_S$ scale. *Geophys. J. Roy. Astr. Soc.* **28**, 431–458.

McCloskey, J., Nalbant, S.S., Steacy, S. (2005). Earthquake risk from co-seismic stress. *Nature* **434**, 291.

Milder, D.M. (1969). Ray and wave invariants for SOFAR channel propagation. *J. Acoust. Soc. Amer.* **46**, 1259–1263.

Milne, A.R. (1959). Comparison of spectra of an earthquake $T$ phase with similar signals from nuclear explosions. *Bull. Seismol. Soc. Amer.* **49**, 317–329.

Munk, W.H. (1979). Sound channel in an exponentially stratified ocean with applications to SOFAR. *J. Acoust. Soc. Amer.* **55**, 220–255.

Munk, W.H., Spindel, R.C., Baggeroer, A., Birdsall, T.G. (1994). The Heard Island feasibility test. *J. Acoust. Soc. Amer.* **96**, 2330–2342.

Nábělek, J., Xia, G. (1995). Moment-tensor analysis using regional data; application to the 25 March 1993, Scotts Mills, Oregon earthquake. *Geophys. Res. Lett.* **22**, 13–16.

Newman, A.V., Okal, E.A. (1998). Teleseismic estimates of radiated seismic energy: The $E/M_0$ discriminant for tsunami earthquakes. *J. Geophys. Res.* **103**, 26885–26898.

Norris, R.A., Johnson, R.H. (1969). Submarine volcanic eruptions recently located in the Pacific by SOFAR hydrophones. *J. Geophys. Res.* **74**, 650–664.

Northrop, J. (1974). $T$ phases from the Hawaiian earthquake of April 26, 1973. *J. Geophys. Res.* **79**, 5478–5481.

Northrop, J., Menard, H.W., Duennebier, F.K. (1968). Seismic and bathymetric evidence of a fracture zone on Gorda Ridge. *Science* **161**, 688–690.

Occhipinti, G., Lognonné, P., Kherani, A., Hébert, H. (2005). Modeling and detection of ionospheric perturbation associated with the Sumatra tsunami of December 26th, 2004. *Eos, Trans. Amer. Geophys. Un.* **86** (52), U11A-0829 (abstract).

Odom, R.I. (1986). A coupled mode examination of irregular waveguides including the continuum spectrum. *Geophys. J. Roy. Astr. Soc.* **86**, 425–453.

Odom, R.I., Soukup, D.J. (2004). Model scattering of $T$ waves: Sediment amplification and source effects. *J. Acoust. Soc. Amer.* **115**, 2445 (abstract).

Officer, C.B. (1958). Introduction to the Theory of Sound Transmission, with Application to the Ocean. McGraw-Hill, New York, 284 pp.

Ogata, Y. (1983). Estimation of the parameters of the modified Omori formula for aftershocks frequencies by the maximum likelihood procedure. *J. Phys. Earth* **31**, 115–124.

Ohrnberger, M., Krüger, F. (2005). Imaging of large earthquake rupture processes using multiple tele-seismic arrays: Application to the Sumatra–Andaman Islands earthquake. *Eos, Trans. Amer. Geophys. Un.* **86** (52), U11A-819 (abstract).

Okal, E.A. (1982). Higher moment excitation of normal modes and surface waves. *J. Phys. Earth* **30**, 1–31.

Okal, E.A. (1988). Seismic parameters controlling far-field tsunami amplitudes: A review. *Natural Hazards* **1**, 67–96.

Okal, E.A. (2001a). $T$-phase stations for the international monitoring system of the comprehensive nuclear-test ban treaty: A global perspective. *Seismol. Res. Lett.* **72**, 186–196.

Okal, E.A. (2001b). "Detached" deep earthquakes: Are they really?. *Phys. Earth Planet. Inter.* **127**, 109–143.

Okal, E.A. (2003). $T$ waves from the 1998 Papua New Guinea earthquake and its aftershocks: Timing the tsunamigenic slump. *Pure Appl. Geophys.* **160**, 1843–1863.

Okal, E.A. (2004). Comment on "Source of the great tsunami of 1 April 1946: a landslide in the upper Aleutian forearc", by G.J. Fryer *et al.*. *Marine Geology* **209**, 363–369.

Okal, E.A. (2007). Seismic records of the 2004 Sumatra and other tsunamis: A quantitative study. *Pure Appl. Geophys.* **164**, 325–353.

Okal, E.A., Kirby, S.H. (2002). Energy-to-moment ratios for damaging intraslab earthquakes: Preliminary results on a few case studies. USGS Open File Rept., 02–328, pp. 127–131.

Okal, E.A., Langenhorst, A.R. (2000). Seismic properties of the Eltanin Transform System, South Pacific. *Phys. Earth Planet. Inter.* **119**, 185–208.

Okal, E.A., Talandier, J. (1981). Dispersion of one-second Rayleigh modes through oceanic sediments following shallow earthquakes in the southcentral Pacific Ocean basin. In: Kuperman, W.A., Jensen, K.B. (Eds.), *Bottom-Interacting Ocean Acoustics*. In: *NATO Confer. Ser.*, vol. IV:5. Plenum, New York, pp. 345–358.

Okal, E.A., Talandier, J. (1986). $T$-wave duration, magnitudes and seismic moment of an earthquake; application to tsunami warning. *J. Phys. Earth* **34**, 19–42.

Okal, E.A., Talandier, J. (1997). $T$ waves from the great 1994 Bolivian deep earthquake in relation to channeling of $S$ wave energy up the slab. *J. Geophys. Res.* **102**, 27421–27437.

Okal, E.A., Talandier, J. (1998). Correction to "$T$ waves from the great 1994 Bolivian deep earthquake in relation to channeling of $S$ wave energy up the slab". *J. Geophys. Res.* **103**, 2793–2794.

Okal, E.A., Dengler, L., Araya, S., Borrero, J.C., Gomer, B., Koshimura, S., Laos, G., Olcese, D., Ortiz, M., Swensson, M., Titov, V.V., Vegas, F. (2002). A field survey of the Camana, Peru tsunami of June 23, 2001. *Seismol. Res. Lett.* **73**, 904–917.

Okal, E.A., Alasset, P.-J., Hyvernaud, O., Schindelé, F. (2003). The deficient $T$ waves of tsunami earthquakes. *Geophys. J. Int.* **152**, 416–432.

Park, M., Odom, R.I. (1999). The effect of stochastic rough interfaces on coupled-mode elastic waves. *Geophys. J. Roy. Astr. Soc.* **136**, 123–143.

Park, M., Odom, R.I., Soukup, D.J. (2001). Modal scattering: A key to understanding oceanic $T$ waves. *Geophys. Res. Lett.* **28**, 3401–3404.

Pasyanos, M.E., Romanowicz, B.A. (1997). Observations of $T$ phases across Northern California using the Berkeley digital seismic network. *Eos, Trans. Amer. Geophys. Un.* **78** (46), 461–462 (abstract).

Pedersen, M.A. (1969). Theory of the axial ray. *J. Acoust. Soc. Amer.* **45**, 157–176.

Pekeris, C.L. (1948). Theory of propagation of explosive sound in shallow water. *Geol. Soc. Amer. Mem.* **27**. Part 2, 117 pp.

Pierce, A.D. (1965). Extension of the method of normal modes to sound propagation in an almost stratified medium. *J. Acoust. Soc. Amer.* **37**, 19–27.

Polet, Y., Kanamori, H. (2000). Shallow subduction zone earthquakes and their tsunamigenic potential. *Geophys. J. Int.* **142**, 684–702.

Press, F., Ewing, W.M. (1950). Propagation of explosive sound in a liquid layer overlying a semi-infinite elastic solid. *Geophysics* **15**, 426–446.

Ravet, J. (1940). Remarques sur quelques enregistrements d'ondes à très courte période au cours de tremblements de terre lointains à l'observatoire du Faiere, Papeete, Tahiti. In: Sixth Pacific Congr., vol. 1, pp. 127–130.

Real, C.R., Teng, T.–L. (1973). Local Richter magnitude and total signal duration in Southern California. *Bull. Seismol. Soc. Amer.* **63**, 1809–1827.

Reymond, D., Hyvernaud, O., Talandier, J., Okal, E.A. (2003). $T$-wave detection of two underwater explosions off Hawaii on April 13, 2000. *Bull. Seismol. Soc. Amer.* **93**, 804–816.

Reymond, D., Hyvernaud, O., Talandier, J., Okal, E.A. (2004). Detection and identification of two anomalous events on the Big Island of Hawaii from teleseismic $T$ phases. *Eos, Trans. Amer. Geophys. Un.* **85** (28), WP112 (abstract).

Reysenbach de Haan, F.W. (1966). Listening under water: thoughts on sound and cetacean hearing. In: Schevill, W.E. (Ed.), *The Whale Problem: A Status Report*. Univ. California Press, Berkeley, pp. 583–596.

Rozenberg, L.D. (1949). Ob odnom novom yavlenii v gidroakustike. *Dokl. Akad. Nauk SSSR* **69**, 175–176 (in Russian).

Saito, M. (1967). Excitation of free oscillations and surface waves by a point source in a vertically heterogeneous Earth. *J. Geophys. Res.* **72**, 3689–3699.

Satake, K., Bourgeois, J., Abe, Ka., Abe, Ku., Tsuji, Y., Imamura, F., Iio, Y., Katao, H., Noguera , E., Estrada, F. (1993). Tsunami field survey of the 1992 Nicaragua earthquake. *Eos, Trans. Amer. Geophys. Un.* **74**, 145 and 156–157.

Scharroo, R., Smith, W.H.F., Titov, V.V., Arcas, D. (2005). Observing the Indian Ocean tsunami with satellite altimetry. *Geophys. Res. Abstr.* **7**, 230 (abstract).

Schmidt, H., Baggeroer, A.B., Sperry, B.J. (2004). Wave-theory modeling of oceanic $T$-phase coupling at continental margin and seamounts. *J. Acoust. Soc. Amer.* **115**, 2444 (abstract).

Scholte, J.G.J. (1947). The range of existence of Rayleigh and Stoneley waves. *Mon. Not. Roy. Astr. Soc., Geophys. Supp.* **5**, 120–126.

Shevchenko, V.V. (1962). Irregular acoustic waveguides. *Sov. Phys. Acoust.* **7**, 389–397.

Shurbet, D.H. (1955). Bermuda *T* phases with large continental paths. *Bull. Seismol. Soc. Amer.* **45**, 23–35.

Shurbet, D.H., Ewing, W.M. (1957). *T* phases at Bermuda and transformation of elastic waves. *Bull. Seismol. Soc. Amer.* **47**, 251–262.

Smith, D.K., Tolstoy, M., Fox, C.G., Bohnenstiehl, D.R., Matsumoto, H., Fowler, M.J. (2002). Hydroacoustic monitoring of seismicity at the slow-spreading Mid-Atlantic Ridge. *Geophys. Res. Lett.* **29** (11), 131–134.

Smith, D.K., Escartin, J., Cannat, M., Tolstoy, M., Fox, C.G., Bohnenstiehl, D.R., Bazin, S. (2003). Spatial and temporal distribution of seismicity along the northern Mid-Atlantic Ridge (15°–35°N). *J. Geophys. Res.* **108** (B3), EPM8-1–EPM8-22.

Stafford, K.M., Fox, C.G., Clark, D.S. (1998). Long-range acoustic detection and localization of blue whale calls in the Northeast Pacific Ocean. *J. Acoust. Soc. Amer.* **104**, 3616–3625.

Stein, S., Okal, E.A. (2005). Size and speed of the Sumatra earthquake. *Nature* **434**, 581–582.

Sverdrup, H.U., Johnson, M.W., Fleming, R.H. (1942). The Oceans, Their Physics, Chemistry and General Biology. Prentice-Hall, New York, 1087 pp.

Swainson, O.W. (1936). Velocity and ray paths of sound waves in sea water. *U.S. Coast Geod. Surv. Field Eng. Bull.* **10**, 64 pp.

Synolakis, C.E., Bardet, J.-P., Borrero, J.C., Davies, H.L., Okal, E.A., Silver, E.A., Sweet, S., Tappin , D.R. (2002). The slump origin of the 1998 Papua New Guinea tsunami. *Proc. Roy. Soc. (London) Ser. A* **458**, 763–789.

Talandier, J. (1966). Contribution à la prévision des tsunamis. *C. R. Acad Sci. Paris B* **263**, 940–942.

Talandier, J., Okal, E.A. (1979). Human perception of *T* waves: the June 22, 1977 Tonga earthquake felt on Tahiti. *Bull. Seismol. Soc. Amer.* **69**, 1475–1486.

Talandier, J., Okal, E.A. (1982). Crises sismiques au volcan Macdonald (Océan Pacifique Sud). *C. R. Acad. Sci. Paris, Sér. II.* **295**, 195–200.

Talandier, J., Okal, E.A. (1987). Seismic detection of underwater volcanism: the example of French Polynesia. *Pure Appl. Geophys.* **125**, 919–950.

Talandier, J., Okal, E.A. (1989). An algorithm for automated tsunami warning in French Polynesia, based on mantle magnitudes. *Bull. Seismol. Soc. Amer.* **79**, 1177–1193.

Talandier, J., Okal, E.A. (1996). Monochromatic *T* waves from underwater volcanoes in the Pacific Ocean: Ringing witnesses to geyser processes?. *Bull. Seismol. Soc. Amer.* **86**, 1529–1544.

Talandier, J., Okal, E.A. (1998). On the mechanism of conversion of seismic waves to and from *T* waves in the vicinity of island shores. *Bull. Seismol. Soc. Amer.* **88**, 621–632.

Talandier, J., Okal, E.A. (2001). Identification criteria for sources of *T* waves recorded in French Polynesia. *Pure Appl. Geophys.* **158**, 567–603.

Talandier, J., Okal, E.A. (2004a). Hydroacoustic signals from presumed CHASE explosions off Vancouver Island in 1969–70: A modern perspective. *Seismol. Res. Lett.* **75**, 188–198.

Talandier, J., Okal, E.A. (2004b). Amplitude-duration and other discriminants for seismically recorded hydroacoustic phases. *Eos, Trans. Amer. Geophys. Un.* **85** (47), F1297 (abstract).

Talandier, J., Hyvernaud, O., Okal, E.A., Piserchia, P.-F. (2002). Long-range detection of hydroacoustic signals from large icebergs in the Ross Sea, Antarctica. *Earth Planet Sci. Lett.* **203**, 519–534.

Talandier, J., Hyvernaud, O., Reymond, D., Okal, E.A. (2006). Hydroacoustic signals generated by parked and drifting icebergs in the Southern Indian and Pacific Oceans. *Geophys. J. Int.* **165**, 817–834.

Tanioka, Y., Ruff, L.J., Satake, K. (1997). What controls the lateral variation of large earthquake occurrence along the Japan Trench?. *The Island Arc* **6**, 261–266.

Tanioka, Y., Satake, K. (1996). Fault parameters of the 1896 Sanriku tsunami earthquake estimated from tsunami numerical modeling. *Geophys. Res. Lett.* **23**, 1549–1552.

Teague, W.J., Carron, M.J., Hogan, P.J. (1990). A comparison between the generalized digital environmental model and Levitus climatologies. *J. Geophys. Res.* **95**, 7167–7183.

Thorp, W.H. (1965). Deep ocean sound attenuation in the sub- and low-kilocycle per second region. *J. Acoust. Soc. Amer.* **38**, 648–654.

Tindle, C.T. (1979). The equivalence of bottom loss and mode attenuation per cycle in underwater acoustics. *J. Acoust. Soc. Amer.* **66**, 250–255.

Tolstoy, L., Clay, C.S. (1966). Ocean Acoustics: Theory and Experiment in Underwater Acoustics. McGraw-Hill, New York, 293 pp.

Tolstoy, L., Ewing, W.M. (1950). The $T$ phase of shallow-focus earthquakes. *Bull. Seismol. Soc. Amer.* **40**, 25–52.

Tolstoy, M., Bohnenstiehl, D.R. (2005). Hydroacoustic constraints on the rupture duration, length, and speed of the great Sumatra–Andaman earthquake. *Seismol. Res. Lett.* **76**, 419–425.

Tsai, V.C., Nettles, M., Ekström, G., Dziewoński, A.M. (2005). Multiple CMT source analysis of the 2004 Sumatra earthquake. *Geophys. Res. Lett.* **32** (17), L17304, 4 pp.

Tsuji, Y., Imamura, F., Matsutomi, H., Synolakis, C.E., Nang, P.T., Jumadi, Harada, S., Han, S.S., Arai, K., Cook, B. (1995). Field survey of the East Java tsunami of June 3, 1994. *Pure Appl. Geophys.* **144**, 839–854.

Urick, R.J. (1963). Low-frequency sound attenuation in the deep ocean. *J. Acoust. Soc. Amer.* **35**, 1413–1422.

Urick, R.J. (1966). Long-range deep-sea attenuation measurement. *J. Acoust. Soc. Amer.* **39**, 904–906.

Urick, R.J. (1975). Principles of Underwater Sound, 2nd ed. McGraw-Hill, New York. 384 pp.

Wadati, K. (1960). On the $T$ phases observed at Torishima. *Geophys. Mag.* **30**, 1–18.

Wadati, K., Inouye, W. (1953). On the $T$ phase of seismic waves observed in Japan. *Proc. Japan Acad.* **29**, 47–54.

Walker, D.A. (1989). Seismicity of the interiors of plates in the Pacific Basin. *Eos, Trans. Amer. Geophys. Un.* **70**, 1543–1544.

Walker, D.A., Bernard, E.N. (1993). Comparison of $T$-phase spectra and tsunami amplitudes for tsunamigenic and other earthquakes. *J. Geophys. Res.* **98**, 12557–12565.

Walker, D.A., McCreery, C.S., Hiyoshi, Y. (1992). $T$-phase spectra, seismic moments, and tsunamigenesis. *Bull. Seismol. Soc. Amer.* **82**, 1275–1305.

Walker, K.T., Ishii, M., Shearer, P.M. (2005). Rupture details of the 28 March 2005 Sumatra $M_W = 8.6$ earthquake imaged with teleseismic $P$ waves. *Geophys. Res. Lett.* **32** (24), L24303, 4 pp.

Wallace, T.C., Koper, K.D. (2002). Forensic analysis of seismic events in the water: submarines, explosions and impacts. *Eos, Trans. Amer. Geophys. Un.* **83** (47), F1049 (abstract).

Ward, S.N. (1980). Relationship of tsunami generation and an earthquake source. *J. Phys. Earth* **28**, 441–474.

Weigel, W. (1990). Bericht über die SONNE-Expedition SO65-2, Papeete–Papeete, 7.-28. Dez. 1989. Universität Hamburg, Institut für Geophysik.

Weinstein, S.A., Okal, E.A. (2005). The mantle wave magnitude $M_m$ and the slowness parameter $\Theta$: Five years of real-time use in the context of tsunami warning. *Bull. Seismol. Soc. Amer.* **95**, 779–799.

Wessel, P., Smith, W.H.F. (1991). Free software helps map and display data. *Eos, Trans. Amer. Un.* **72**, 441 and 445–446.

Wilkinson, J.H. (1965). The Algebraic Eigenvalue Problem. Clarendon Press, Oxford, 662 pp.

Worzel, J.L., Ewing, W.M. (1948). Explosion sounds in shallow water. *Geol. Soc. Amer. Mem.* **27**, Part 1, 63 pp.

Wysession, M.E., Okal, E.A., Miller, K.L. (1991). Intraplate seismicity of the Pacific Basin, 1913–1988. *Pure Appl. Geophys.* **135**, 261–359.

Yang, Y., Forsyth, D.W. (2003). Improving epicentral and magnitude estimation of earthquakes from $T$ phases by considering the excitation function. *Bull. Seismol. Soc. Amer.* **93**, 2106–2122.

Yuan, X., Kind, R., Pedersen, H.A. (2005). Seismic monitoring of the Indian Ocean tsunami. *Geophys. Res. Lett.* **32** (15), L15308, 4 pp.